VIRAL ENCEPHALITIS: PHENOTYPING LEUKOCYTE INFILTRATION INTO THE CENTRAL NERVOUS SYSTEM AS A RESULT OF RIFT VALLEY FEVER VIRUS INFECTION

by

Joseph Robert Albe

BS Microbiology, University of Pittsburgh, 2015

Submitted to the Graduate Faculty of

the Department of Infectious Diseases and Microbiology

Graduate School of Public Health in partial fulfillment

of the requirements for the degree of

Master of Public Health

University of Pittsburgh

2017

UNIVERSITY OF PITTSBURGH

Graduate School of Public Health

This thesis was presented

by

Joseph R. Albe

It was defended on

April 13th, 2017

and approved by

Committee Member:
Douglas S. Reed, PhD
Associate Professor
Department of Immunology
School of Medicine
University of Pittsburgh

Committee Member:
Robbie B. Mailliard, PhD
Associate Professor
Department of Infectious Diseases and Microbiology
Graduate School of Public Health
University of Pittsburgh

Committee Chair:
Amy L. Hartman, PhD
Associate Professor
Department of Infectious Diseases and Microbiology
Graduate School of Public Health
University of Pittsburgh

Amy L. Hartman, PhD

VIRAL ENCEPHALITIS: PHENOTYPING LEUKOCYTE INFILTRATION INTO THE CENTRAL NERVOUS SYSTEM AS A RESULT OF RIFT VALLEY FEVER VIRUS INFECTION

Joseph R. Albe, MPH

University of Pittsburgh, 2017

ABSTRACT

Rift Valley Fever Virus (RVFV) is a vector-borne infection endemic to the Horne of Africa; However, outbreaks in the Arabian Peninsula in 2001 demonstrate its expanding range. Humans can develop encephalitis as a result of RVFV infection. Our lab uses an immunocompetent Lewis rat model to study neuropathogenesis of RVFV. With this model, Lewis rats uniformly develop lethal encephalitis within 7 – 8 days after aerosol exposure. In contrast, Lewis rats infected subcutaneously do not develop apparent disease except at very high doses. The public health significance of RVFV is that it has the potential to natural spread throughout the world and it could be used as a potential bioweapon. The goal of this study is to characterize the phenotypes, timing, and extent of immune cell infiltrate into the CNS of RVFV-infected Lewis rats. Lewis rats were infected with RVFV ZH501 by aerosol or subcutaneous routes, and subsequently serially-sacrificed between 1 and 7 days post infection. Rat immune cells were isolated from brains via percoll gradients, stained with the appropriate antibodies, run on a BD LSRII flow cytometer, and analyzed with FlowJo 7.6.5.

In aerosol-infected rats, the leukocyte infiltrate 5 days post infection and later consisted of primarily neutrophils, corresponding to the clinical window. Despite no apparent disease, rats infected subcutaneously had detectable infiltrate primarily consisting of phenotypic CD4+ T cells.

These findings suggest that aerosol-infected rats mainly exhibit innate leukocyte infiltration to the brain while subcutaneous have limited leukocyte infiltration and display a stronger adaptive immune response. The relative contributions of viral cytopathology versus immunopathology remain to be determined, but this study represent the first attempt to characterize the leukocytic component of RVFV neurological disease.

TABLE OF CONTENTS

LIST OF TABLES

LIST OF FIGURES

PREFACE

I would like to thank Dr. Amy Hartman for all the help and support she has given me throughout this project. There are a number of colleagues and friends who are also responsible for assisting me in this project, who made this all possible.

1.0   INTRODUCTION

1.1   VIRAL ENCEPHALITIS

Encephalitis is the inflammation into the central nervous system (CNS) including the parenchyma as well as the meninges. The etiological agents of encephalitis are generally derived from either infectious agents or autoimmune disease. On a global scale, encephalitis is caused primarily by viral pathogens, such as Japanese Encephalitis Virus (JEV) and Herpes Simplex Virus (HSV) [1]. These viruses pose a conundrum for the immune system, where it must respond to eliminate the viral insult while not causing irreparable damage to the neuronal network and function. In a healthy individual, the CNS is considered an immune privileged site with almost no immune activity beyond surveillance for potential damage by resident cells [2, 3]. Safeguards against immune activation in the CNS include primary antigen presentation outside the CNS in the cervical lymph nodes [3], low levels/no MHC I expression on healthy neuronal cells [4], expression of FAS ligand by many CNS cells to prevent cytotoxic T cell activity [5], and the blood brain barrier (BBB) separation from circulation. However, during viral encephalitis these healthy immune suppressive mechanisms are suspended by the detection of viral replication, leading to leukocyte infiltration to the CNS. The pathways of viral encephalitis are varied, based on viral tropism, host functions, and the route of entry to the CNS, and therefore are complicated to study

as a general phenomenon. Herein, viral entry and host barriers to the CNS are reviewed as well as host immune responses to viral insults within the CNS.

1.1.1 Viral Blood-Brain Barrier interactions for entry to CNS

Viral entry to the CNS is poorly understood for many viruses. The BBB is known to play an integral role in regulating entry to the CNS (2). The BBB is a multi-layered endothelial cell membrane that is joined together through tight-junctions, effectively separating circulation from the CNS vasculature. This membrane is maintained by various resident immune cells that prevent biological insults. Astrocytes play a disproportionate role in the maintenance and phenotype of the BBB through physical contact with the endothelial cells and secretion of cytokines (6). However, viruses have evolved several mechanisms by which to subvert this physical barrier and gain entry to the CNS, despite the many regulatory cells.

The first two mechanisms utilize the BBB's own selectivity to gain CNS entry. One mechanism of this type is through direct attachment to BBB cellular markers, by the virus and facilitated entry in the endothelial cells, as seen with Epstein-Bar Virus (EBV) (7, 8). This mechanism is not without cost as the direct infection of the endothelial cells can induce an antiviral state, through production of type I interferons (IFN) and limit viral replication (8). Another mechanism is through infected leukocyte migration in to the CNS, also known as the "Trojan Horse (7)." Many lentiviruses utilize this method of entry to the CNS by infecting monocytes in the periphery, which replicate increasing peripheral viral loads (9). Eventually, the infected monocyte interacts with the BBB and undergoes transmigration. This successfully allows the virus to pass through the BBB without direct viral interaction with the endothelial layers. These two

methods utilize the BBB's own markers to pass through, whether through direct interaction or an intermediary.

The other two mechanisms avoid the BBB by using peripheral neurons to reach the CNS. The first of this type of mechanism is through the utilization of sensory neurons as seen with HSV (10). HSV infection initially takes place in epithelial cells and subsequently infects an innervating sensory neuron where it can eventually reach the CNS(10). Since sensory neurons are part of the peripheral nervous system (PNS), they are not protected by the BBB. Once in the sensory neuron the virus is retro-trafficked to the basal ganglia where it may enter the CNS through synaptic connections (10). The second mechanism of entry of this type is through motor neurons. While HSV can also enter through this mechanism other viruses exclusively use this mechanism, such as rabies virus. This utilizes the same means that HSV does in sensory neurons, but with motor neurons (7). These peripheral neurons are not without their own protective immune cells, which help pose an additional barrier to undetected viral entry to the neurons and CNS.

Whichever entry mechanism is used by a virus, BBB integrity can be depleted and can cause breakdown. It has been demonstrated that matrix metalloproteinase-9 (MMP-9) is upregulated during acute brain injury and leads to BBB breakdown (11). MMP-9 is also known to be upregulated in JEV through simulation of the NFkB pathway astrocytes from viral presentation (12). BBB integrity can also be decreased due to direct viral replication and subsequent damage (8). Regardless of how the BBB integrity is decreased, leukocytes are able to enter the CNS from the periphery in response to viral replication, leading to viral encephalitis.

1.1.2 Host Response

The response of the host to the viral insults widely varies between viruses for several reasons, including the viral lifecycle. DNA viruses have a nuclear phase and can often go latent in the CNS, which can have the byproduct of immune evasion for the virus. Alternatively, RNA viruses typically do not have a nuclear phase and are more likely to cause acute viral infection. For the purposes of this paper only RNA virus host responses will be discussed.

The host immune response must attempt to balance effective viral elimination and neuronal network damage once virus has entered the CNS. IFNs are important components of the innate factors produced by host cells in response to viral infections. It has previously been thought that type 1 IFNs (IFN-1) were responsible for viral responses; it is now known that this is not correct and that both type 1 and type 2 IFNs have important roles in viral responses (13). However, the parenchyma of the brain lacks typical peripheral cells that produce IFNs during active viral encephalitis (13). It was recently found that despite neuronal suppression of IκBα by gangliosides, neurons are able to produce IFNs during early infection in an NFκB-independent manner (13, 14). Neurons and glial cells are able to produce IFNs and induce an innate antiviral state, slowing viral replication so that an adaptive response may be mounted. Viruses often target IFNs/IFN-producing pathways to prevent hindrance to their replication, such as NSs protein in *Bunyaviruses (15)* or NS2A protein of the *Flaviviruses (16)*.

Glial cells are also important in the early response of the CNS to viral infection. Microglia and astrocytes are important immune functioning glial cells that initiate local responses and begin recruitment of peripheral leukocytes to the parenchyma of the brain through cytokine production. Microglia are the self-renewing resident macrophage population that serve as the sentinel

surveillance system of the CNS (17). Microglia are also one of the only cells to express MHC II in the parenchyma of the brain and are largely responsible for the limited antigen presentation that takes place within the CNS (2, 18). For these reasons, microglia are imperative to the initial immune response in the CNS to viral infection and the ensuing neuroinflammation.

Both neurons and glial cells, chiefly microglia, send neurotropic chemokines to the periphery. This causes the infiltration of T lymphocytes, B cells, monocytes, natural killer cells and granulocytes into the CNS. Many of these cells, such as antigenspecific T lymphocytes and monocytes, can transmigrate through an intact BBB (19). Monocytes can enter the CNS through the BBB where they can replenish depleted microglia (20-22). Conversely, there have been reports that the monocyte population cannot be distinguished from the microglial populations by extracellular markers. The replenished microglia phenotype could be monocytes that have entered due to the breakdown of the BBB and are not actually replenishing the microglial population (23). Therefore, to distinguish between microglia and monocytes, one must normally obtain additional information beyond extracellular markers. Monocytes are often found in the brain early during infection but this is not always the case. Under certain viral encephalitic conditions, neutrophils have been known to cross the BBB during early infection (24). During transmigration of the BBB, neutrophils decrease the BBB vascular integrity, likely through MMP-dependent mechanisms (24). Therefore, neutrophils during early infection tend to be more associated with reduced BBB integrity, and thus more immune infiltrate. B and T cells infiltrate once an adaptive response can be mounted and assist in viral clearance or suppression.

Reduction in the integrity of the BBB presents a question for those who study viral encephalitis: does the pathogenesis come from viral lysis/budding and resulting destruction of tissue, from the immune response to the infection, or both? Semliki Forest Virus (SFV) represents

an example of neurological disease as a strict result of the immune response. In SFV mouse models, it was determined that the virus infiltrates the CNS and the mice uniformly develop neurological disease through demyelination of the neurons. However, upon the depletion of CD8+ cytotoxic cells from the mice, there was no brain pathology, despite viral replication (25). Conversely, some viruses can directly infect neurons where they can lead to apoptosis or necrosis, damaging neuronal networks. In order to understand the viral encephalitis and for the rational development of treatments as well as vaccines, this etiology of neurological disease should be known to insure efficacy.

1.2   RIFT VALLEY FEVER VIRUS

1.2.1   Epidemiology

Rift Valley Fever Virus (RVFV) is an arbovirus and member of *phlebovirdae,* endemic to most of Africa and since 2001 portions of the Middle East (26). Primarily RVFV is carried and spread through the *Aedes* mosquitos, but has been demonstrated to be transmitted through several arthropod vectors, including flies and ticks (26). In endemic regions RVFV is maintained in enzootic cycles where mosquitos interact with wild ungulates and allow the virus to continue circulating in low levels (27, 28). During these enzootic cycles, desiccated mosquito eggs are cable of harboring virus for years, leading to infected progeny after egg activation (26, 29). In the epizootic cycle, eggs hatch during the rainy season and the resulting progeny expand infectivity beyond wild ungulates and into domesticated ruminants as well as humans (30).

6

Infection in domestic ruminants can result in what is known as 'abortion storms,' where many pregnant animals have spontaneous abortions, a unique clinical feature of RVFV (26). While initial infection of these animals begins with vector transmission, interaction with infected tissue can result in transmission and amplification of the epizootic cycle (31). During epizootic outbreaks, human transmission can come from directly handling infected tissue, or animal product such as unpasteurized milk (31). While most of the human cases are asymptomatic, outbreaks have shown symptoms including ocular, neurologic, and hemorrhagic manifestations (31). While these symptoms are relatively rare, the results from ocular, hemorrhagic, or neurologic disease can have a lifetime impact on the individual who succumbs to the illness. Furthermore, many of those who are most at risk, shepherds and farmers, can be put out of work due to the illness and be unable to carry on their livelihood. Miscarriages have also recently been linked with human RVFV infection (32). This new finding is troubling, as many of the epizootic outbreaks in humans have been on a moderate scale, rarely impacting more than a few hundred people. However, should RVFV outbreak occur on a more global scale, something in the scale of a Zika or West Nile Virus outbreak, the result could potentially wipe out a generation.

1.2.2 Public Health Significance

Recent expansion of RVFV into the Arabian Peninsula in 2001 has shown that the virus is capable of spreading into new regions, particularly given the warming climate (33). Today, the Americas, Europe, and most of Asia remain free of this virus. However, zika, dengue,, and West Nile viruses have all demonstrated that arboviruses are more than capable of spreading globally, where they can lead to dramatic disease and sequelae. RVFV is no different than these other arbovirus, and the threat, in the case of RVFV, should be taken more seriously due to the potential

for infection and subsequent devastation of livestock, along with humans. Due to the aforementioned 'abortion storms' caused in domesticated ruminants as well as miscarriages and variety of diseases in humans, the spread of RVFV to a naïve area, could severely deplete the food supply as well as strain medical capabilities. The possibly of spread to naïve areas is more feasible than ever with globalized trade, travel and a warming global climate.

In addition to natural spread of the virus, RVFV has been labeled as a potential bioweapon due to ease of infection from inhalation (34). This route of transmission has been demonstrated before in several laboratories. Whether released purposefully or accidentally, RVFV would be difficult to recognize in a naïve population, and would spread rapidly as RVFV is promiscuous in the number of vectors that can spread it. Therefore, RVFV represents a significant and ever increasing threat to the modern world and its economy.

1.2.3 Virology

RVFV is a tripartite negative single stranded RNA virus. The segments of the genome are straightforwardly known as long (L), medium (M), and short (S) segments. The virion enters the cell through the binding of viral glycoproteins Gn and Gc to heparan sulfate and induce endocytosis, though the exact mechanism remains unknown (35). In a pH-dependent manner, the virus membrane fuses with the endosome membrane and the virus is able to escape destruction and begin the replication cycle. The L segment codes for a RNA-dependent RNA polymerase for viral transcription. The L segment is also capable of cap snatching to propagate the translation of the viral genome by host machinery (36). The M segment responsible for nonstructural protein (NSm) and the two glycoproteins (Gn and Gc) that are found on the envelope of the complete viral particle. The S segment is ambisense and codes for the second nonstructural protein (NSs) in the

positive polarity and in the negative polarity, the N protein. Viral assembly occurs in a localize area of the cell, and the virus utilizes the endomembrane system for a lipid bilayer to egress from the cell.

NSs is a key player in the viral immune evasion. NSs has been shown to block IFNs, particularly IFNs-1 in in vitro as well as in vivo models in a NFkB and IRF-3 independent fashion, as these are still activated during infection (37). Without the NSs protein, the virus is attenuated due to a robust immune response through type I interferons (IFN). However, in Protein Kinases RNA-activated (PKR) deficient cells, a virus deficient in NSs retained pathogenicity, indicating that RVFV specifically targets the dsRNA recognition molecule and ubiquinates it for degradation. In addition to targeting the host viral sensor, RVFV also suppresses IFN-beta transcripts directly. It does this by forming a NSs homodimer which can then polymerize into a filament and interaction with Sin3A Associated Protein 30 (SAP30) (38). The interaction between NSs filament and SAP30 causes histone rearrangement of the IFN gene, effectively silencing any transcriptional expression (38). It is believed that silencing is also done through the degradation of the p62 component of the pre-initiator complex for host polymerase II (15, 39).

NSm also is utilized by RVFV as an immune evasion protein. NSm is made from the M segment and the initial translation of the segment yields a polyprotein, which is cleaved by host proteases into NSm1 and NSm2. NSm1 protein has been demonstrated to function as a direct inhibitor of caspase 8 induced apoptosis through mitochondrial localization and modulation with reactive oxygen species (40). Additionally, NSm1 has been associated with inhibition of caspase 9 and 3, though the mechanism for these remains unknown (40). The NSm2 has a unique function from NSm1, but may act as a surrogate for NSm1 (41). However, when the NSm sequence is removed from of the virus, the virus is unable to replicate in monocytes, whereas a single mutation

in either allows for the infection of monocytes (41). While it is not yet understood why this mutation results in poor monocyte infection, it demonstrates that NSm plays a role in evasion and survival of the virus in the host.

1.2.4   Animal Model

Several models for RVFV have been developed for studying each of the disease states (febrile, ocular, hemorrhagic, and neurological). For neurological disease, an immunocompetent Lewis rat model has been developed when it is exposed through aerosol (AERO). When immunocompetent Lewis rats are exposed to AERO RVFV the mortality is 100% after 8 days of infection with as low as 10^3 PFU (42). This model has also demonstrated that the site of viral replication is in the brain tissue, as confirmed by plaque assay and PCR (42, 43). Subcutaneous (SC) RVFV exposed immunocompetent Lewis rats do not succumb to death and do not exhibit any apparent neurological disease after infection with the same strain of virus (42, 44). This makes immunocompetent Lewis rats an ideal candidate for understanding neurological disease, as exposure route determines a reliably uniform clinical disease.

In the early stages of infection, 0 to 4 days post infection (dpi) in this model, there is transient viral replication in the periphery and no overt disease symptoms (43). The clinical window for AERO infection begins at 5 dpi until death, usually on day 7 or 8. The clinical window is determined when the animal becomes symptomatic, such as hunching of the back or rolling. Within this clinical window, weight loss, fever, decreased activity, altered posture, and perforin staining around eye, nose and mouth can be observed (43). Virus can be detected at low levels in the brain within 24 hours after infection. Virus titers increase exponentially, reaching 10^6-10^8 pfu/g during the clinical window (5-7 dpi) (43). Pathological changes in the brain, indicating

encephalitis, can be seen as early as 4 dpi. The pathology also showed apoptosis of neural structures, vasculitis, and morphological neutrophils and other infiltrating leukocytes (43). Also corresponding with the beginning of the clinical window were spikes in several cytokines including, MCP-1, RANTES, IL-18 and interferon gamma.

In the periphery, there was viral replication detected in several organs, as early as 1 dpi with AERO exposure (43). Many of the cytokines seen in the brain were also seen in the peripheral response, but at earlier time points, chiefly 4 dpi. RANTES was an exception, which had biphasic modulation at both 1 and 5 dpi (43). Complete blood counts (CBC) were performed and demonstrated a continuous increase in granulocytes and thrombocytopenia. However, lymphocytes differed, with a biphasic modulation in serum at 1 and 5 dpi.

Together the viral load and corresponding immune response paint a picture of systemic infection and later infiltration of cells into the brain to match the onset of neurological symptoms. The importance of the cells infiltrating the CNS is currently a topic that is unknown, but imperative if the neurological disease of RVFV is to be understood. Without a thorough understanding of the neurologic disease, effective therapeutics, vaccines, and clinical indicators will be difficult to develop. Moreover, RVFV neurological disease will also be nearly impossible to determine from other encephalitic viruses. For these reasons, we seek to understand the differences in immune cell infiltration to the CNS during both SC and AERO infection, to compare leukocyte phenotypes that may elucidate the discrepancies seen in the overt diseases of both routes.

2.0   SPECIFIC AIMS

2.1   PROJECT STATEMENT

The neurological disease caused by Rift Valley Fever Virus (RVFV) is poorly understood in all models. Our lab uses an immunocompetent Lewis rat model study the neurological component of RVFV. Lewis rats develop uniformly lethal encephalitis within 7 days after AERO exposure to RVFV. Conversely, Lewis rats injected SC with RVFV do not develop disease. During viral encephalitis, it is not well understood if neurological disease and subsequent death, as in the AERO-infected Lewis rats, is a result of virus-triggered cell death or an adherent immune response. One of the steps towards understanding the etiological cause of disease in AERO-infected rats is to compare the immune infiltrate of the central nervous system (CNS) to non-neurological disease infection, the SC-infection route. Additionally, neurological disease may be symptomatic of a systemic response, leading to eventual immune infiltration of the CNS. For this reason, it is important to also phenotype the leukocytes that are present in the circulation of both AERO- and SC-infected rats.

The goal of these studies is to determine the phenotype of resident and infiltrating immune cells into the CNS, through flow cytometry, in order to better understand the nuances between SC and AERO infection for future testing of therapeutics in RVFV. It is also important in our attempt to understand how the peripheral immune response may correlate with encephalitis. Our hypothesis is that AERO exposed immunocompetent rats will exhibit large amounts of leukocyte infiltration near 5dpi while SC exposed will exhibit little or no leukocyte infiltration through the duration of the study.

2.2   PROJECT SPECIFIC AIMS

Specific Aim 1: To determine the phenotype, timing, and extent of immune cell infiltrate to the central nervous system (CNS) of Lewis rats infected with RVFV by either SC or AERO routes.

A. Using flow cytometry, the infiltration of leukocytes to the CNS after either AERO or SC infection will be compared over time based on extracellular markers.

B. Using flow cytometry to study specific microglial and neutrophil populations in the CNS through the course of infection and to include earlier and later time points of infections.

Specific Aim 2: To compare phenotypes of peripheral immune cells and how they relate to the observed phenotypes in the CNS as a result of infection with RVFV by either SC or AERO routes.

A. Changes in blood derived leukocyte populations after either AERO or SC infection will also be compared to better understand systemic response prior to CNS infiltration using flow cytometry methods

3.0   METHODS

3.1   ANIMAL INFORMATION

Female immunocompetent Lewis rats were used in all time courses. These rats were between 8 and 10 weeks old. All rat studies were conducted under IUCUC approval, using number 14125012.

3.2   VIRUS INFORMATION

All infections of immunocompetent Lewis rats utilized Rift Valley Fever Virus (RVFV) ZH501. This strain was provided by Barry Miller and Stuart Nichol from Center for Disease Control, Atlanta, GA. This virus is considered a Select Agent and was handled according to the biosafety specifications listed within this section. Virus was propagated in VeroE6 cells utilizing standard cell culture methods.

3.3   BIOSAFETY

All studies were conducted in the Regional Biocontainment Laboratory (RBL) at the Center for Vaccine Research (CVR) within the University of Pittsburgh. This facility is registered with the CDC/USDA for work with RVFV. All infected tissue handling was done at biosafety level 3 (BSL-3) environment and proper personal protective equipment was utilized. Samples that

were taken out of BSL-3 conditions were inactivated overnight (at least 12 hours) using 4% paraformaldehyde (PFA). In the RBL all infected samples were handled under a class II biological safety cabinet. Any waste generated was autoclaved prior to removal and any surfaces that came into contact with infected samples were disinfected with Vesphene II.

3.4   ANIMAL INFECTION

3.4.1   Aerosol

All aerosol infections were performed by Dr. Douglas Reed and his lab. Rats received an average inhaled dose of $3\text{x}10^4$ plaque-forming units (PFU) of ZH501 RVFV through an Aeroneb nebulizer (Aerogen, Inc, Chicago, IL) controlled by the Biaera AeroMP exposure system (Biaera Technologies, Hagerstown, MD). Rats were exposed to aerosols for 10 minutes in a whole-body chamber located inside a class III biosafety cabinet. Aerosol samples were collected during exposures in liquid media inside an all-glass impinger which was used to determine the delivered inhaled dose using a plaque assay.

3.4.2   Subcutaneous

All subcutaneous (SC) (under the skin) infections were performed by Aaron Walters. Lewis rats were exposed to Isoflurane (USP NDC 11695-0500-2) in a drop container to induce general anesthesia. Rats were then exposed to dose of 500uL of 1.00E+06 ZH501 RVFV by SC injection. All SC infections were done using the hind legs of rats.

3.5   STUDY DESIGN

For each time course, female immunocompetent Lewis rats were randomized into uninfected control, SC ZH501 exposure, or AERO ZH501 exposure groups. Each ZH501 exposure type were randomly assigned into day of sacrifice groups. Rats were serial sacrificed between 0 and 7 days' post infection (DPI). For AERO, if exposed rats met euthanasia criteria prior to designated day of sacrifice, they were sacrificed on that day. For aim1a 2 SC-infected rats and 4AERO-infect rats were sacrificed for each day. For aim1b 3 SC-infected rats and 3 AERO-infected rats were sacrificed for each day.

3.6   BRAIN CELL ISOLATION

Following euthanasia, each Lewis rat was perfused and brain extracted for cell isolation. Brains were stored in Hanks Buffer Salt Solution without calcium or magnesium (HBSS w/o) (Sigma H9394) until processing could be performed. Whole brains were then divided into hemispheres, covered with 1mL of digestion buffer, consisting of 10mg/ml DNase I (Sigma 10104159001), 20mg/ml of collagenase (Sigma C2674-500mg), and 6.75mL of HBSS w/o. The sample was then chopped using a scalpel and covered with an additional 6.5mL of digestion buffer. The sample was then incubated at 37C for 45 minutes, with repeated agitation, using a transfer pipette, every 15 minutes to generate a homogenous liquid. Once the sample was a homogenous

16

liquid, it was filtered using a 40uM strainer. The remaining homogenate was then suspended in

12mL of wash buffer, consisting of 150uL of DNase I and 30.5ml HBSS with 3% fetal bovine

serum (FBS). The solution was then centrifuged at 500 x gravity for 8 minutes at room temperature.

The supernatant was then removed and the pellet suspended in an additional 18mL of wash buffer

and centrifuged at 500 x gravity for 8 minutes at room temperature. Supernatant was then removed

and the remaining pellet suspended in an 80% Percoll (Sigma GE17-0891-01), suspended in HBSS

solution. The suspended pellet is then layers with 38% and 21% Percoll and topped with HBSS

with 3% FBS. The Percoll gradient separates cell types by density and leukocytes, during

centrifugation at 480 x gravity for 35 minutes, move to the third interface, that between the 80%

and 21%. The third interface was extracted and suspended in 30mL HBS w/o with 3% FBS and

centrifuged for 8 minutes at 300 x gravity. The supernatant was removed and the pellet was washed

with 10mL of HBS w/o with 3% FBS. The supernatant was again discarded and the remaining

pellet suspended in 1 ml FACS buffer. Cells were then counted and placed on ice until it could be

stained. This protocol was adapted from isolation of leukocytes in stroke model rats (Figure 1)

(45).
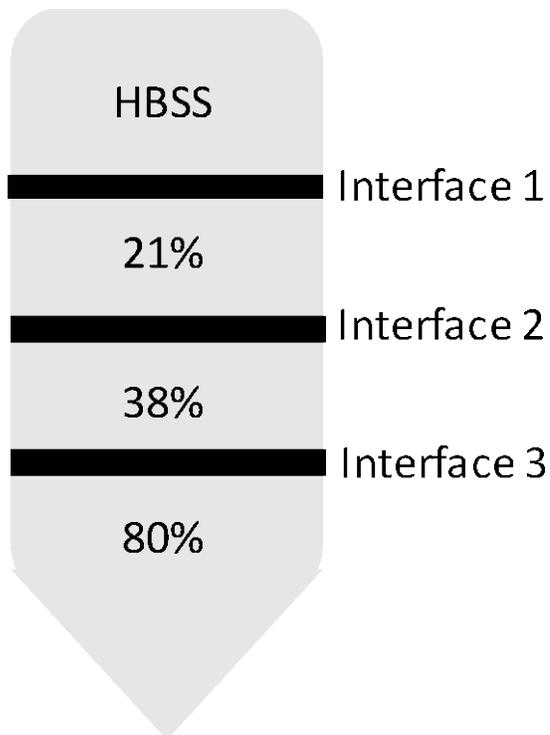
Figure 1. Brain leukocyte isolation gradient using a Percoll gradient.

3.7 STAINING PANELS

CD45 is a tyrosine phosphatase on leukocytes that was used as a pan-leukocyte marker for all panels. CD68 is a lipoprotein binding receptor and is used as a pan-macrophage marker and could be used to identify microglia. CD163 is a scavenger receptor on macrophages and used to identify peripheral/infiltrating macrophages. Iba-1 is an ionized calcium binding molecule that is present on microglia. RP-1 is a rat neutrophil antigen and was thus used to identify neutrophils. CD11b is an integrin protein that can be used to identify microglia when co-localized with CD68 or neutrophils when co-localized to RP-1. CD3 is a generic T lymphocyte marker. CD8 and CD4 were used to identify the subtypes of lymphocytes.

3.8   STAINING PROTOCOLS

For study number R31, three separate panels were used to stain for all tissue samples collected. Each panel was used to determine distinct populations.

Table 1. Staining Panel for R31 experiments (Aim 1a and b).

Neutrophil Panel			Lymphocyte Panel		
Marker	Clone (Format) Company		Marker	Clone (Format) Company	
CD45	OX-1 (V450) BD		CD45	OX-1 (V450) BD	
His-48	His-48 (FITC) BD		CD3	1FA (APC) BD	
RP-1	RP-1 (PE) BD		CD4	OX-35 (PE) BD	
CD11b	WT.5 (APC) BD		CD8	OX-8 (FITC) BD	
Macrophage Panel					
Marker	Clone (Format) Company				
CD45	OX-1 (V450) BD				
CD11b	WT.5 (APC) BD				
CD163	His-36 (PE) BD				
CD68	ED1 (FITC) BIORAD				

For clarification, a second set of experiments was performed in order to ensure proper identification of microglia and neutrophils. Two additional markers were included, calprotectin,

as a confirmation of RP-1 expression on neutrophils, and Iba-1, to confirm microglia populations beyond CD68 and CD11b co-expression. The panels were also rearranged to ensure that neutrophils were not expressing "monocyte/macrophage," markers (CD68, Iba-1, CD163), and macrophages/monocytes were not expressing "neutrophil markers," (RP-1, Calprotectin)

Table 2. Staining Panel for R34/R35 experiments (Aim 2a and b).

Neutrophil Panel		Macrophage Panel	
Marker	Clone(Format)Company	Marker	Clone(Format)Company
CD45	OX-1 (Pe-Cy7) BD	CD45	OX-1 (Pe-Cy7) BD
RP-1	RP-1 (BV786) BD	RP-1	RP-1 (BV786) BD
CD11b	WT.5 (V450) BD	CD11b	WT.5 (V450) BD
CD163	His-36 (PE) BD	CD163	His-36 (PE) BD
Calprotectin	S100A9(FITC)BIORAD	CD68	ED1(FITC)BIORAD
		Iba-1	EPR6136(2)(Alexa647)ABCAM

3.8.1   Brain Cell staining

Leukocytes suspended in FACS buffer were placed in a V-bottom 96-well plate and centrifuged for 500x gravity for 4 minutes at 4C. A blocking solution, 2uL of anti-CD32 and 18uL of FACS buffer per sample, was added to each sample and the samples incubated for 20 minutes on ice in the dark. Cells were then washed twice with 200uL FACS buffer and a 500x gravity for 4-minute centrifugation and stained with antibodies for 30 minutes on ice in the dark. The stained

samples were then washed twice with 200uL FACS buffer and a 500x gravity for 4-minute centrifugation followed by the addition of 200uL of 4% PFA for overnight inactivation.

3.8.2   Whole Blood lysis and staining

Blood is taken from each Lewis rat prior to euthanasia from 0 through 7 days post infection. 50uL of whole blood was taken from each animal and directly stained with the appropriate amount of antibody for 15 minutes. 450uL of FACS lysis buffer was used to lyse red blood cells for 30 minutes. Samples were then washed with FACS buffer and centrifuged for five minutes at 500xgravity, twice. The samples were then inactivated with 500ul of 4% PFA overnight.

3.9   GATING STRATEGY

All samples were run on a BD LSR II and analyzed using Flowjo 7.6.5. All samples initial gate was a vital brain gate used for viability of leukocytes based on side scatter and granularity. All samples were then further refined using a double inclusion using forwards scatter and side scatter to prevent any confounding events. CD45 was then used to identify leukocytes in all samples. Distinction was made to differentiate between high and medium expression of CD45. These two gates served the parent gate for all subsequent gates shown.

4.0   RESULTS

4.1   SPECIFIC AIM 1

4.1.1   Specific Aim 1A

In order to determine the timing, phenotype, and extent of immune infiltration, a serial sacrifice experiment was performed after rats were exposed to RVFV ZH501 through either AERO or SC routes. Three rats were euthanized daily from 3 to 6 days post infection (dpi), where peripheral blood and CNS infiltrate were analyzed using flow cytometry.

Samples were run on BD LSRII flow cytometer, and analyzed using Flowjo 7.6.5. Initial analysis of all of brain samples was done using a vital brain gate that is used to determine viable immune cells based on side scatter and granularity (Figure 2A) (45). These events were further gated based on side scatter area and height (Figure 2B). This was further gated to reveal CD45 expression versus side scatter (Figure 2C). Previous studies have shown that intermediate CD45 expression (indicated as CD45^{med} in Figure 2C) within the brain can be used to crudely identify resting microglia (45). Similarly, CD45^{high} expression can be used to identify infiltrating leukocytes or activated microglia that have increased their expression of CD45 (Figure 2C).
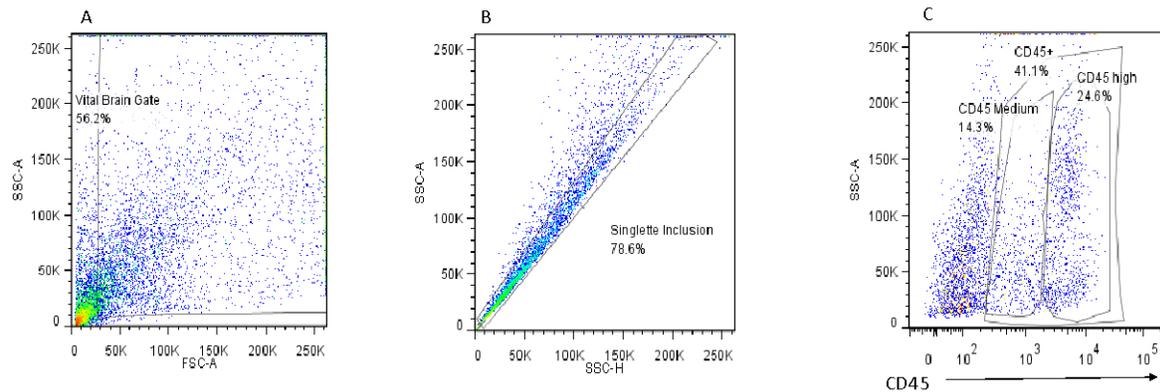
Figure 2. Flow cytometry gating strategy on vital brain and singlet inclusion in AERO RVFV infected Lewis rat brain.

Sample gating strategy from 6 dpi in AERO infected Lewis rat. **A)** Vital brain gate based on forward and side scatter for viable brain cells. **B)** Singlet inclusion to avoid any events that could give false associations of markers based on complexity. **C)** CD45+ vs SSC-A to distinguish leukocytes from other cells and debris.

The expression of CD45, regardless of medium or high, can be used to determine number of leukocytes within each tissue sample based on total cell counts using a hemocytometer. Significant increases in total isolated cells were observed with AERO-infected throughout the time course, indicating cell infiltration, while SC-infected remained at control levels of leukocytes (Figure 3).

23
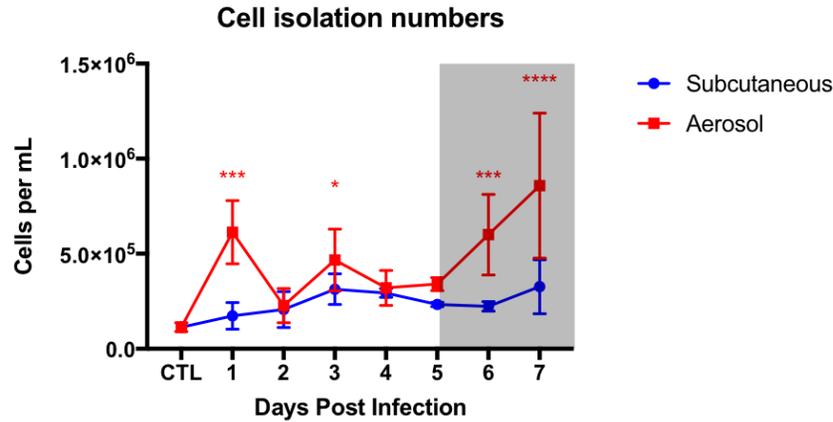
Figure 3. Number of leukocyte density cells isolated from brain samples after RVFV infection.
Hemocytometer was used to calculate these values. Data taken from aim 1b. For illustrative purposes is displayed in aim 1a. $P < 0.05$ *, $P < 0.01$ **, $P < 0.001$ ***, $P < 0.0001$ ****

As expected, flow cytometry indicated that in the brain of uninfected Lewis rats, most CD45+ cells were resting microglia (Figure 4A). In AERO-infected rats on 6 dpi, there was a notable population of CD45^{hi} cells not seen in uninfected rats (Figure 4C). Surprisingly, there was also a small increase in CD45^{hi} cells in SC-infected rats on 6 dpi. In the brains of AERO-infected rats there was an increase into the proportion of activated microglia/infiltrating leukocytes and concurrent decline in resting microglia at the onset of the clinical window (5 dpi), suggesting that these changes coincide with the clinical manifestations (Figure 5). Conversely, in the brains of SC-infected rats there was a decrease in resting microglia and no significant change in activated microglia/infiltrating leukocytes (Figure 5). This suggests resting microglia are decreasing in both AERO- and SC-infected rats, but only AERO-infected rats experience an increase in CD45^{high} cells which could be either infiltrating leukocytes or activated microglia. It is curious that AERO-infected rats which develop lethal encephalitis have increased numbers of CD45hi leukocytes in the brain, while SC-infected rats which survive without apparent disease do not have the same

24

increase of CD45hi leukocytes. This finding suggests AERO-infected rats have more immune infiltrate or activated microglia in the CNS than the SC-infected.
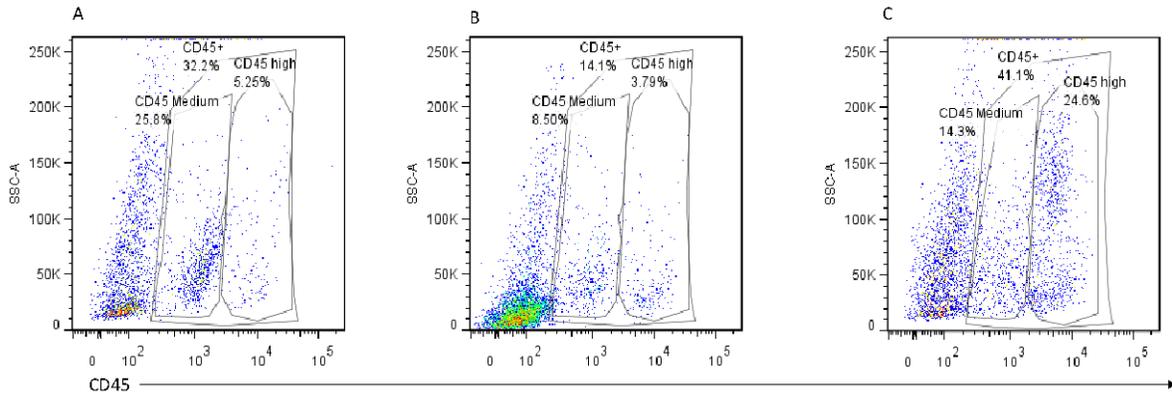
Figure 4. Flow cytometry gating strategy for crude identification of microglia and leukocyte infiltrate in RVFV infected Lew rat brain.

All data gated on vital brain gate and singlet inclusion as in Figure 2. CD45^{medium} crudely represent microglia. CD45^{high} represent activated microglia or infiltrating leukocytes. All data was based on CD45+ populations **A)** Uninfected Lewis rat (control (CTL) **B)** 6dpi SC-infected rat **C)** 6 dpi AERO-infected rat
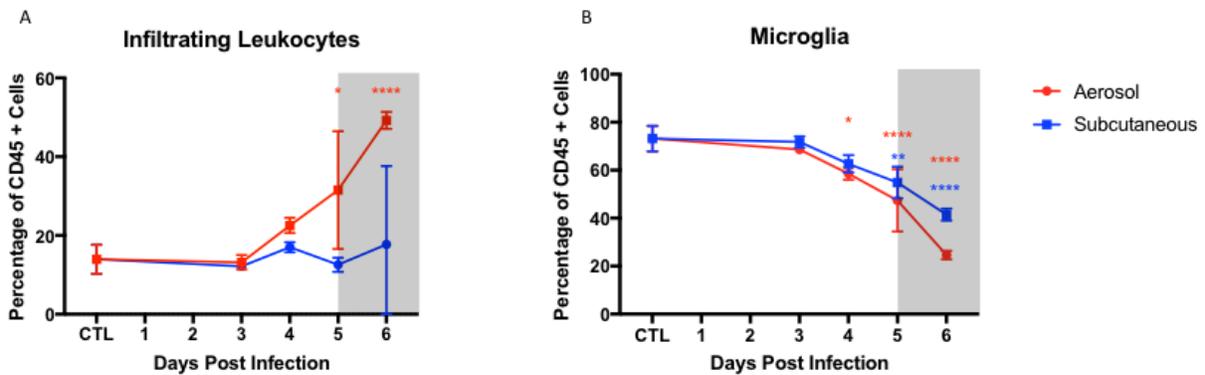
Figure 5. Number of leukocytes in RVFV-infected rats based on CD45 expression and infection route.

$P < 0.05 = *$, $P < 0.01$ **, $P < 0.001$ ***, $P < 0.0001$ **** Legend indicates route of infection with RVFV.
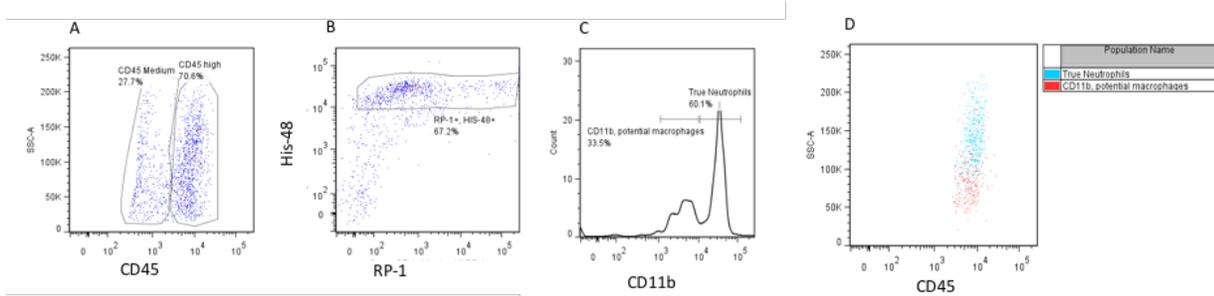
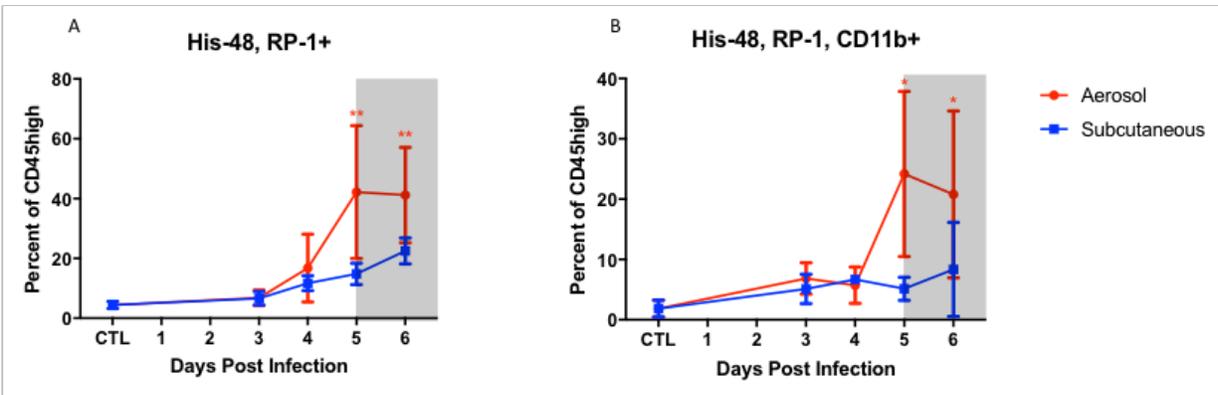**Figure 6. Neutrophil gating strategy for RVFV infected Lewis rat brain.**

A) Represents two CD45 expression versus side scatter. Gated on CD45^{high} **B)** CD45^{high} His-48, and RP-1 expression. **C)** Histogram showing D11b expression on His-48+, RP-1+ gated cells indicating two distinct populations. **D)** Placement of the distinct CD11b populations based on SSC property and CD45 expression.

Further gating of CD45^{high} cells allowed identification of this population, which based on side scatter, could be lymphocytes, granulocytes or myeloid cells (Figure 6A). In rats, all granulocytes should express CD45 at high levels and should also express His-48, a rat pan-granulocyte antigen. RP-1, a neutrophil antigen in rats, can be further used to define the granulocytes, in addition to CD11b, an integrin subunit. The majority of the CD45^{high} population expressed both His-48 and RP-1 (Fig. 6B). When CD11b^{+} expression of His-48^{+} and RP-1^{+} positive cells was examined, there were two populations, CD11b^{med} and CD11b^{high} (Figure 6C). Additional gating of each population reveal differences in side scatter, with CD11b^{med} events being roughly macrophage side scatterd, while CD11b^{high} events being roughly neutrophil side scatterd (Figure 6D). This could not be definitively determined in this experiment because macrophage markers were used in a separate panel. However, based on CD45^{high}, His-48^{+}, RP-1^{+}, and CD11b^{high} expression, there was anan influx of neutrophils at 5 dpi corresponding with the clinical window seen in AERO-infected rats. In the SC-infected rats, this influx from the control was not seen, and thus neutrophils appear to be a major difference between the two infection routes (Figure 7A-B).
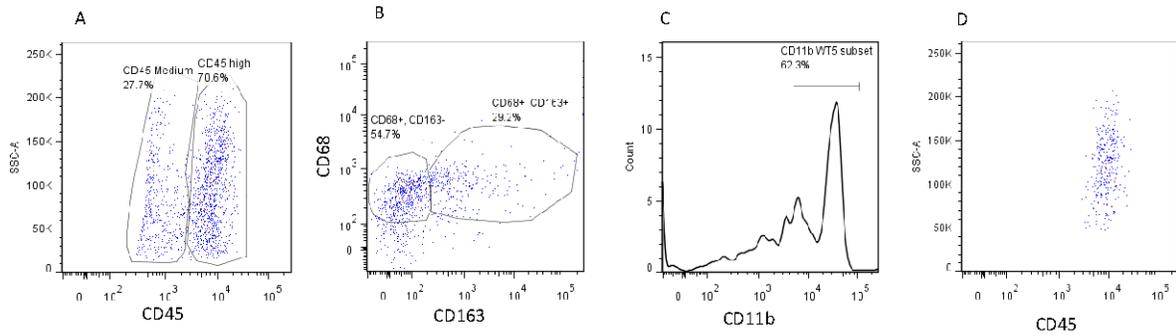
Figure 7. Neutrophil population in CNS by percentage of CD45^{high}.

Data determined through flow cytometry for both SC and AERO infected rats. Gating strategy for this data shown in figure 6. His-48 and RP-1 co-expression can be used to phenotypically distinguish neutrophils. The co-expression of His-48, RP-1, and CD11b is a more rigorous way to identify true neturophils.

P < 0.05 *, P < 0.01 **, P < 0.001 ***, P < 0.0001 ****

Because macrophages are an important target for RVFV infection (41), we attempted to differentiate between infiltrating macrophages and activated microglia, which would both fall within the CD45^{high} gate. In theory, activated microglia should be CD45^{high}, CD68$^+$ (a lysosome activity marker), CD11b$^+$, but should not express CD163 (a scavenger receptor expressed on peripheral macrophages) (Figure 8). Conversely, infiltrating macrophages would be CD45^{high}, CD68$^+$ CD163$^+$. Using differential expression of CD163, there was no significant change in percetnages in activated microglia for either SC or AERO -infected rats compared to control counterparts (Figure 9B). While this finding was no statistically significant, it was suggestive of a trend. Infiltrating macrophages (CD45^{high}, CD68$^+$, CD163$^+$) were increased on 3dpi for both infection routes but then returned to control levels thereafter (Figure 9A).

27

Figure 8. Macrophage gating strategy for CD45 ^{high} leukocytes in RVFV infected Lewis rat brain.

A) Represents two CD45 expression versus side scatter. Gated on CD45^{high}. **B)** CD45^{high} cells by CD163 and CD68. Two populations, CD68+, CD163-, and CD68+, CD163+ double positive. **C)** Gated on CD68+ CD163- population to show CD11b expression to identify microglia. **D)** To show the side scatter and CD45 expression of phenotypic activated microglia.
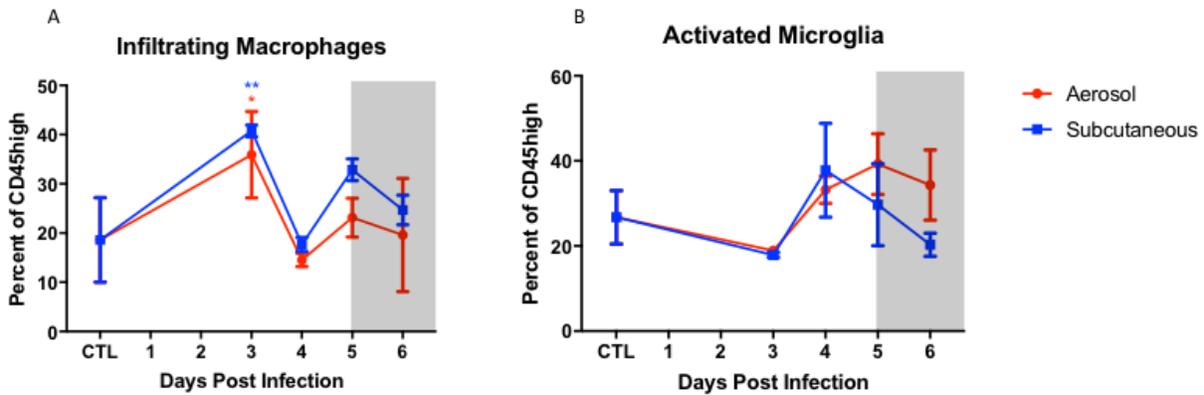
Figure 9. CD45^{high} macrophage/microglia population in CNS by percentage of CD45^{high}.

Data determined through flow cytometry for both SC and AERO infected rats**.** Infiltrating macrophages identified as CD45high, CD68+ and CD163+ double positive (gating shown in figure 8). Activated microglia identified as CD45high, CD68+, CD163-, and CD11b+ (gating shown in figure 8). $P < 0.05$ *, $P < 0.01$ **, $P < 0.001$ ***, $P < 0.0001$ ****

To identify resting microglia and potential replenishing monocytes, we examined the CD45^{med} population (Figure 10). Phenotypically, resting microglia should express CD45^{med},

CD68^{+}, CD11b^{+}, and CD163^{-}. This phenotype was significantly depleted in both infection routes as early as 3dpi and remained until the end of the study (Figure 11 B). Potential replenishing macrophages express CD163^{+} along with CD68^{+} and CD11b^{+}. Only SC-infected rats showed a significant increase in the potential replenishing phenotype on 6dpi as a percentage of CD45^{med}. There was an increase over the time course studied for both routes but this increase was not significant when compared to uninfected controls (p value?) (Figure11A).

Figure 10. Macrophage/microglia gating strategy in CD45^{medium} in RVFV infected Lewis rat brain.

A) Represents two CD45 expression versus side scatter. Gated on CD45^{medium}. **B)** CD45^{medium} cells by CD163 and CD68. Two populations, CD68+, CD163-, and CD68+, CD163+ double positive. **C)** Gated on CD68+ CD163- population to show CD11b expression to identify resting microglia. **D)** To show the side scatter and CD45 expression of phenotypic resting microglia.
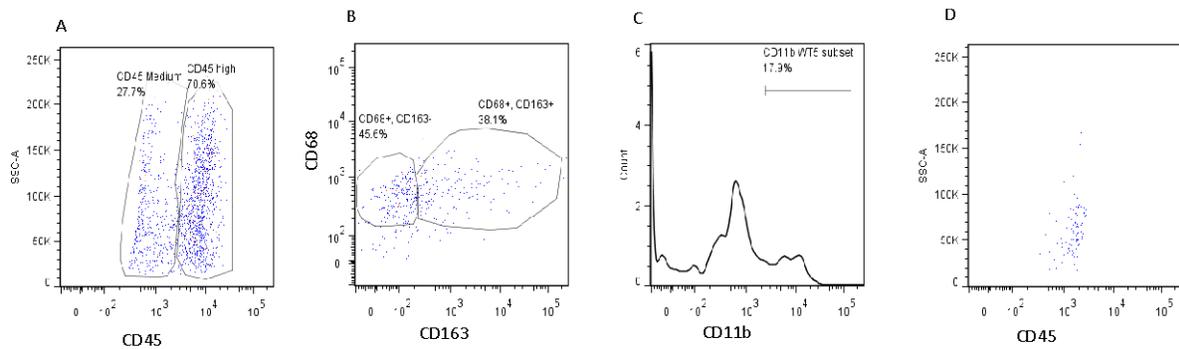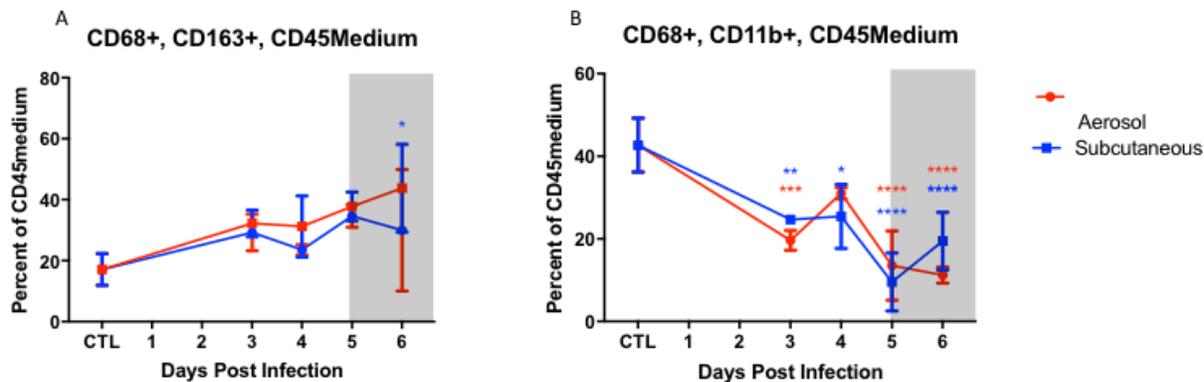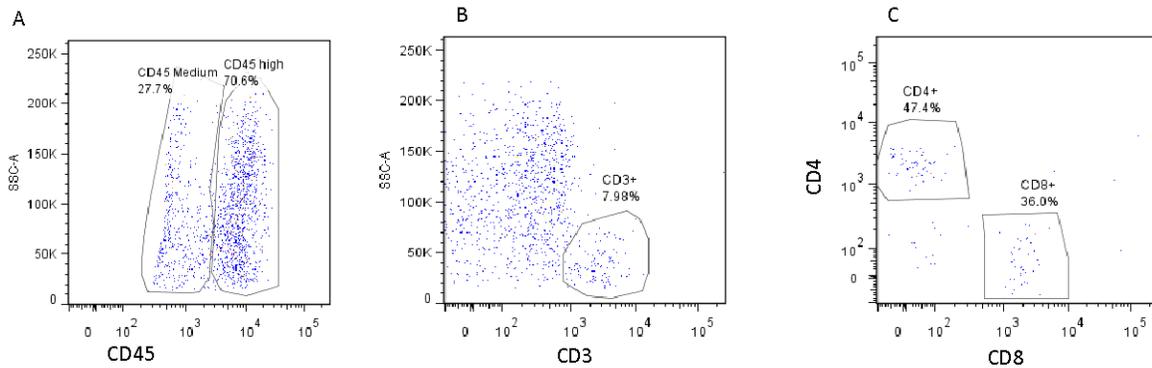
29

Figure 11. CD45^{medium} macrophage/microglia population in CNS by percentage of CD45^{medium}.
Data determined through flow cytometry for both SC and AERO infected rats**.** Gating strategy shown in Figure 10.
A) Presumptive infiltrating macrophages identified as CD45high, CD68 and CD163 double positive. **B)** Potential
resting microglia identified as CD45high, CD68+, CD163-. Resting microglia further refined by CD11b positivity. P
< 0.05 *, P < 0.01 **, P < 0.001 ***, P < 0.0001 ****

While the majority of CD45^{high} cells appeared to be of either granulocyte or monocyte
lineage (Figs. 8,10), we also looked at T lymphocytes. T cells were phenotyped as CD45^{high} and
CD3^{+} (Figure 12A-B). When looking at this population, it increased as a proportion of the CD45^{high}
gate for SC-infected rats starting on 6dpi and, significantly decreases in AERO-infected rats
starting on 5dpi, also corresponding to clinical window (p < .05) (Figure 13A). Further
phenotyping T lymphocytes, CD4^{+} cells express CD45^{high}, CD3+, and CD8- (Figure 12C). These
cells increased as a proportion of the CD45^{high} population at 6dpi in the brains of SC-infected rats
and decreased as a proportion of CD45^{high} population in the brain of AERO-infected rats on 5dpi,
(Figure 13 B-C). For CD8^{+} cells, phenotyped as CD45^{high}, CD3^{+} and CD4^{-}, there was a
proportional decrease starting at 5dpi in the brains of AERO-infected rats. SC-infected rat brains
showed a transient proportional dip in CD8^{+} phenotype events only on 4dpi. (Figure13 B-C). It is

therefore, CD4$^+$ T cells that are responsible for the proportional increase in CD3$^+$ expression in the brains of SC-infected rats, while AERO-infected rats appear to have a proportional decrease in this same population. This is likely due to the influx of neutrophils starting 5dpi for AERO-infected.

Figure 12. T Lymphocyte gating strategy in CD45^{high} in RVFV infected Lewis rat brain.

A) Represents two CD45 expression versus side scatter. Gated on CD4^{high}. **B)** CD45^{high} cells by side scatter and CD3. **C)** Gated on CD3+ for CD8+ and CD4+ populations.
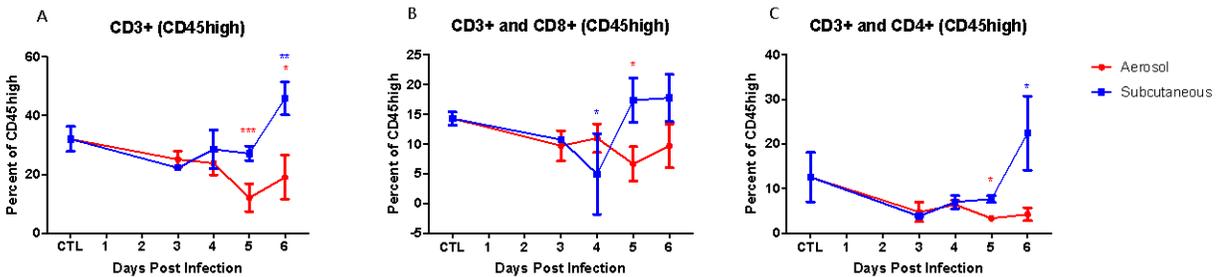
**Figure 13. CD45^{high} T Lymphocyte population in CNS by percentage of CD45^{high}.**

Data determined through flow cytometry for both SC and AERO infected rats. Gating shown in Figure 12. **A)** Represents CD45^{high} CD3+ cells. **B)** represents CD45^{high}, CD3+, and CD8+ cells. **C)** Represents CD45^{high}, CD3+, and CD4+. P < 0.05 = *, P < 0.01 **, P < 0.001 ***, P < 0.0001 ****

31

Overall, it appears that neutrophils are relevant on 5dpi for AERO-infected rats, corresponding to the clinical window observed. Alternatively, SC-infected rats demonstrated a more intermediate response in innate immune cells, but appeared to have a T lymphocyte dominated response compared to the control as well as the AERO-infected animals. It is also possible, that some of the extracellular markers overlap across phenotypes and could cause our results to not add up to 100%.

4.1.2 Specific Aim 1b

In order to get a better scope of the immune cells infiltrating the brain, we next combined our previous panels to understand the phenotypes and their timing in the brain better (Table 2). Here we used new clones of antibodies and different conjugated fluorophores from the previous experiment. This study was used to clarify some of the confounding phenotypes observed in aim 1. The gating strategy shown in Figure 14 A-C was again used. Using a manual hemocytometer we were able to calculate the number of cells in each gate. This allowed for the direct comparison between SC-infected and AERO-infected. Using this method for CD45^{high} and CD45^{med} demonstrated that there were more cells in general in the AERO-infected than the SC-infected, but also that CD45^{med} cells were a significant part (Figure 15).
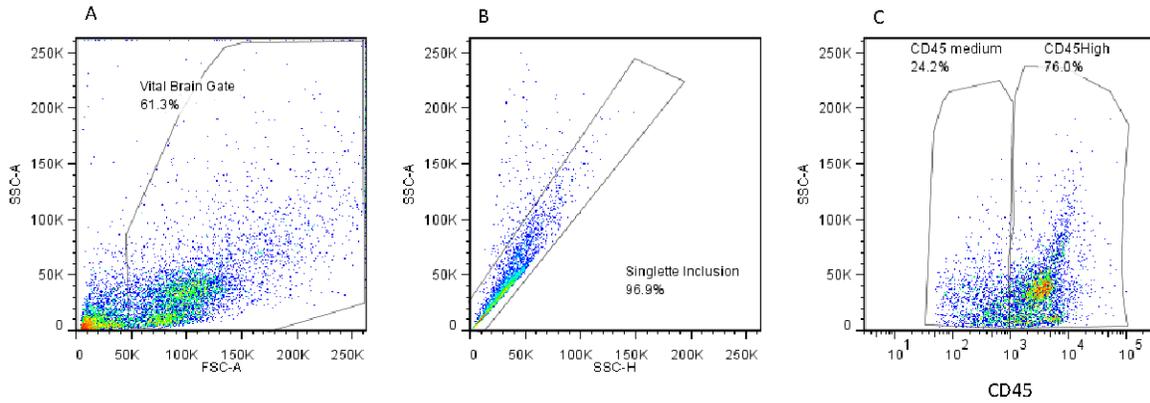
Figure 14. Flow cytometry gating strategy for vital brain and singlet inclusion RVFV infected Lewis rat brain.
Sample gating strategy from 6 dpi in AERO infected Lewis rat. Renewed gating strategy for expanded experiment.
A) Vital brain gate to identify viable brain cells. **B)** Singlet inclusion. **C)** CD45 expression broken down by medium and high expression.
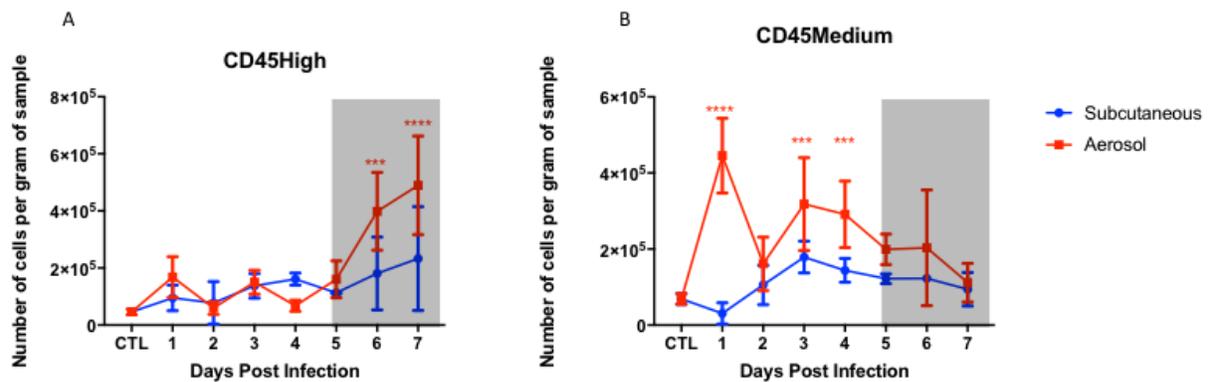
Figure 15. Flow cytometry gating strategy for vital brain and singlet inclusion RVFV infected Lewis rat brain.
Sample gating strategy from 6 dpi in AERO infected Lewis rat. Renewed gating strategy for expanded experiment.
A) Cell count comparison for CD45^{high} in aim1b **B)** Cell count comparison for CD45^{medum}.
$P < 0.05 = *$, $P < 0.01$ **, $P < 0.001$ ***, $P < 0.0001$ ****

For confirmation of activated microglia (using the previously described phenotype of CD45^{high}, CD68$^+$ and CD11b$^{+)}$, we looked at co-expression of a potential microglia-specific marker, Iba-1. We demonstrated that there are two levels of CD11b expression, high and

medium, (Figure 15 A-B), confirming previous results (Figure 6). As suggested by Fig. 6, many

of the events expressing CD11b at high levels did not express Iba-1, indicating that they are

likely not microglia and are indeed likely neutrophils as suggested below (Figure 1616 D).

However, the CD11b^{med} population does express more Iba-1, again confirming these are likely

myeloid cells (Figure 1616 C).
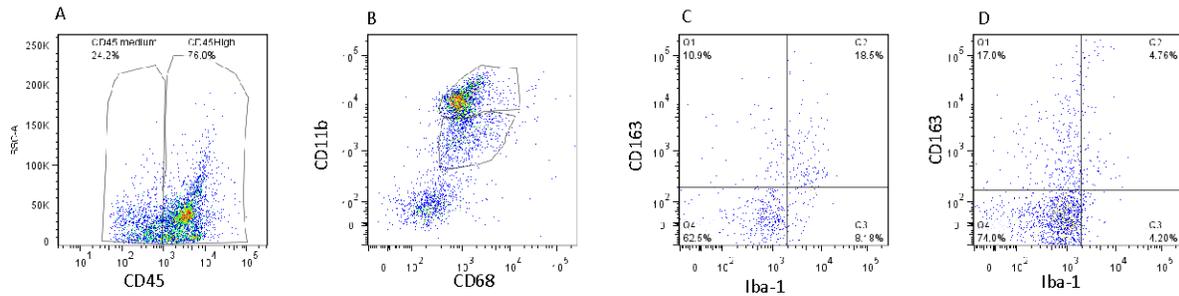
Figure 16. Microglial identification gating strategy for CD45^{high} leukocytes in RVFV infected Lewis rat brain.
All data gated on Vital brain gate and Singlet inclusion. **A)** CD45 positive events broken down into medium and high expression. **B)** CD11b and CD68 on CD45^{high} cells. Two populations gated, CD11b^{high} and CD11b^{medium}. **C)** Expression of CD163 and Iba-1 on CD68+ CD11b^{medium} cells. **D)** CD163 and Iba-1 expression on CD68+ CD11b^{high} cells

Using a similar gating strategy to identify microglia, peripheral macrophages were

evaluated within the CD45^{high} gate for expression of CD163 and Iba-1. These were gated for

CD11b^{+} and CD68^{+} but RP-1^{-} (Figure 1717 A-D). For the CD45^{high} CD163^{+} Iba-1^{+} populations,

we saw depletion from control levels throughout the study for both infection routes (Figure 1818

A). For CD45^{high} CD163^{+} Iba-1^{-} populations we saw mixed decreases and control levels

throughout the time course for both infection routes (Figure 18 B). For all CD45^{med} CD163^{+} we

saw no significant changes from control levels (Figure 18 D-C).

34
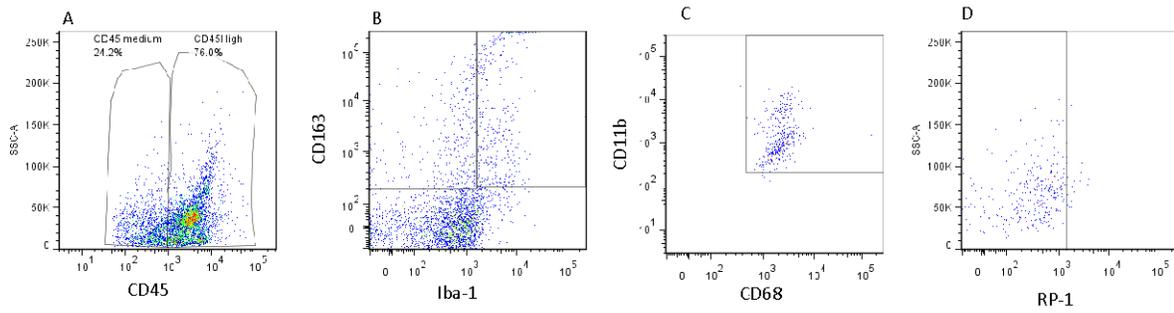
Figure 17. Microglial identification gating strategy for CD45^{high} leukocytes in RVFV infected Lewis rat brain.
A) CD45 positive events broken down into medium and high expression. **B)** Gated on CD45^{high} or CD45^{medium}. CD163 and Iba-1 used to compare microglia and peripheral cells expressing Iba-1. **C)** Gated on either CD163+ Iba-1+ or CD163+ Iba-1- to show CD11b expression and CD68 expression. **D)** Gated on CD68+ CD11b+ to show exclusion of RP-1.
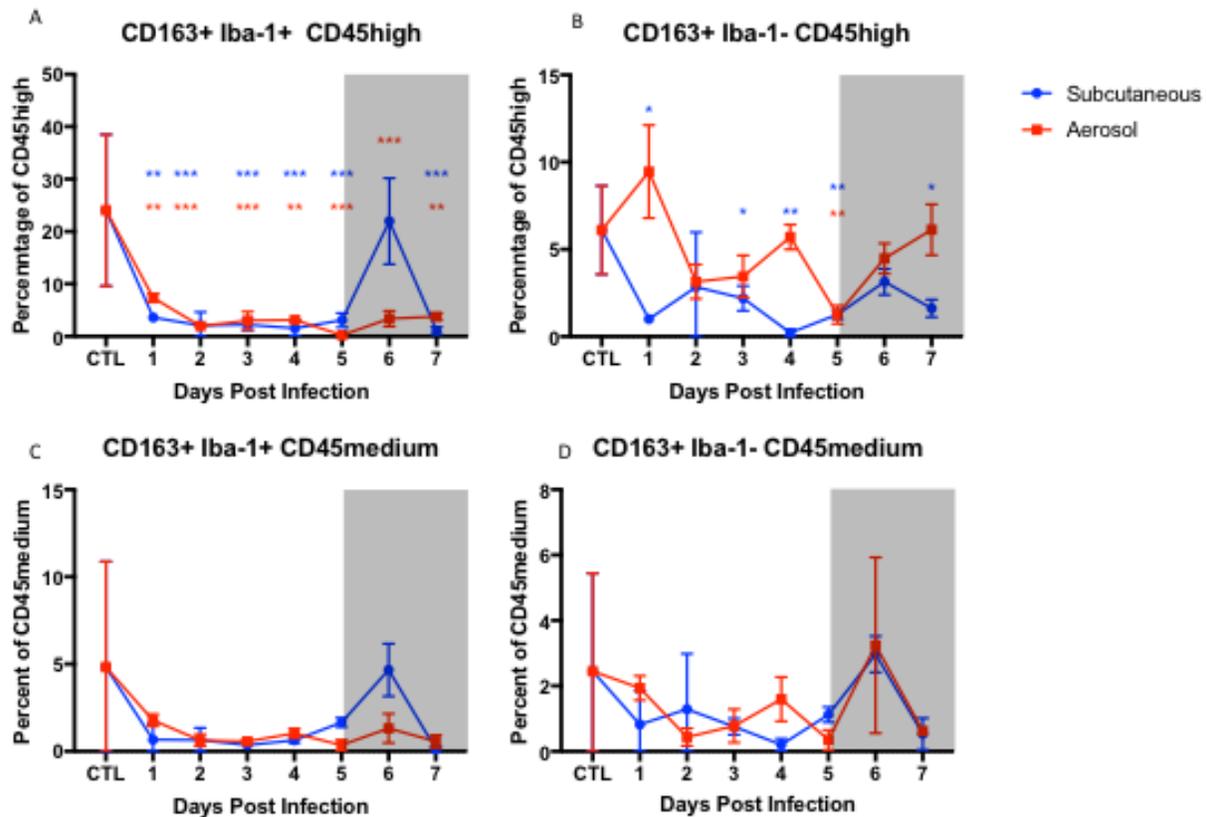
Figure 18. Infiltrating macrophages population in brain as percentage of either CD45^{high} or CD45^{medium}.

Data determined through flow cytometry for both SC and AERO infected rats. Gating shown in figure 16. **A)** CD163+, Iba-1+, CD11b+, CD68+, RP-1- events in the CD45^{high} gate. **B)** CD163+, Iba-1-, CD11b+, CD68+, RP-1- events in the CD45^{high} gate. **C)** CD163+, Iba-1+, CD11b+, CD68+, RP-1- events in the CD45^{medium} gate. **D)** CD163+, Iba-1-, CD11b+, CD68+, RP-1- events in the CD45^{medium} gate. $P < 0.05 = *$, $P < 0.01 **$, $P < 0.001 ***$, $P < 0.0001 ****$

Iba-1 is thought to remain constitutively expressed on microglia, making it a relatively specific microglial phenotypic marker (46). For this reason, we looked at all brain CD45$^+$ cells, both high and medium, and the expression of Iba-1 across infection routes at 5dpi because this correlates to AERO clinical symptoms, (Figure 1919 A-C). Of the Iba-1$^+$ cells, we then looked at their distribution among CD45 expression, and found that many of these positive cells are in the CD45^{med} range, right at the height of infection (Figure 1919 D). Additionally, we looked at Iba-

36

1^{+} cells distribution across CD163^{+}, peripheral macrophage marker, (Figure 1919 E). Here we found that in AERO-infected rats, there is a distinct CD163^{+}, Iba-1^{+} phenotype that neither the SC-infected nor the control exhibits. This could mean that microglia are being replenished from the periphery, as previous studies have shown (20, 21), or could be the presence of peripheral monocytes that are phenotypically indistinguishable from microglia (23). To understand the relative breakdown of microglia phenotype in both CD45 populations, we used the exclusion of CD163^{+} and RP-1^{+}, and the inclusion of CD68^{+}, Iba-1^{+}, and CD11b^{+} (Figure 20 A-D). Overall, phenotypic microglia became depleted in both infection routes and both CD45 expressions (Figure 21 A-B). Interestingly, CD45[med] phenotypic microglia experienced a transient drop and a return to control levels, while AERO-infected only experience the drop (Figure 21 B). Together these data suggest that reduction in microglia could play a role in the neuropathogenisis of AERO-infected rats.
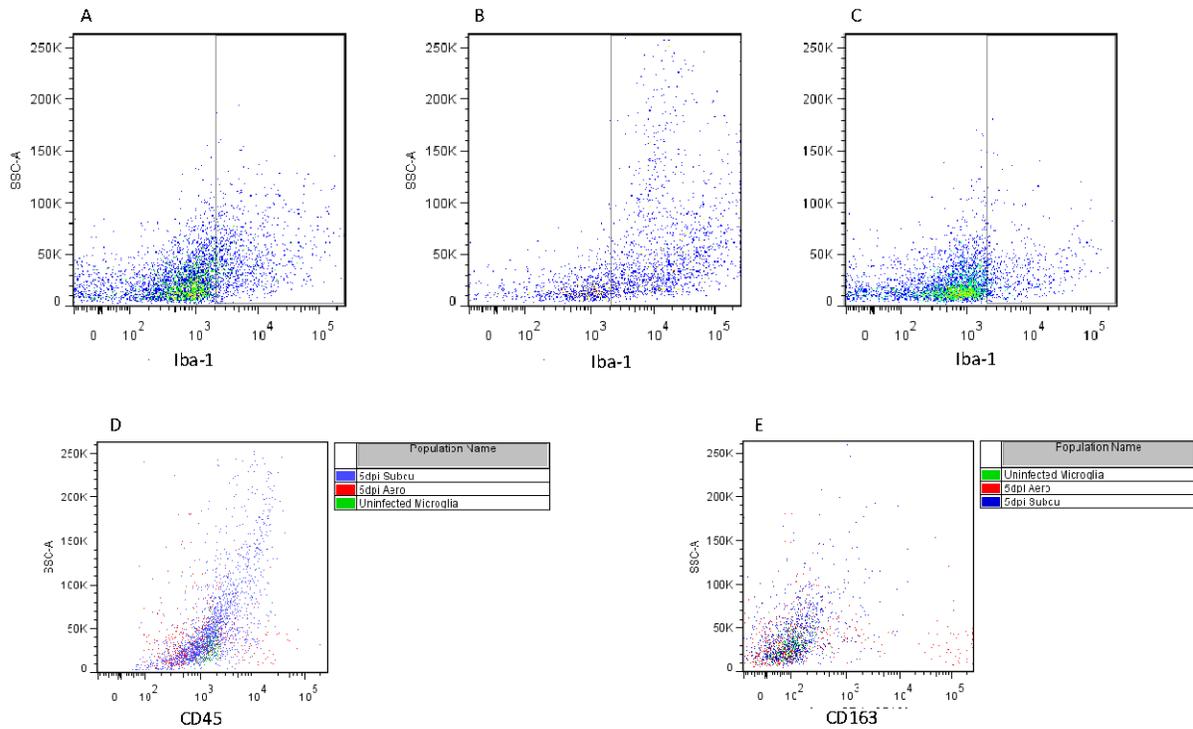
Figure 19. Microglia extracellular expression in infected Lewis rat brain at 5 dpi.

A) Uninfected Lewis rat gated on all CD45 positive events to show Iba-1 expression. **B)** SC Lewis rat gated on all CD45 positive events to show Iba-1 expression. **C)** AERO-infected Lewis rat gated on all CD45 positive events to show Iba-1 expression. **D)** Gated on all CD45, Iba-1 positive events across infections to show CD45 expression. **E)** Gated on all CD45, Iba-1 positive events across infections to show CD163 expression.
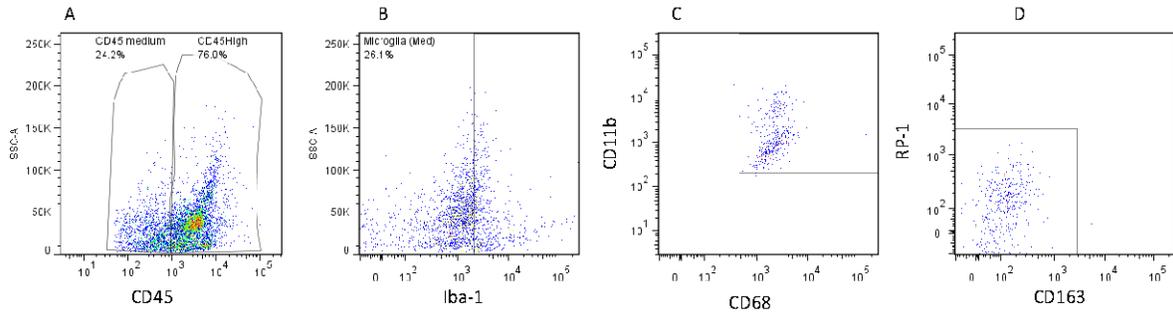
Figure 20. Activated and resting microglia phenotype gating strategy in RVFV infected Lewis rat brain.
All data gated on Vital brain gate and Singlet inclusion. **A)** CD45 positive events broken down into medium and high expression. **B)** Gated on CD45$^{high\ or\ Medium}$ expression to show Iba-1+ population. **C)** Gated on Iba-1+ to show CD68+ CD11b+ **D)** Gated on CD68+ CD11b+ expression to show CD163+ and RP-1+ exclusion.
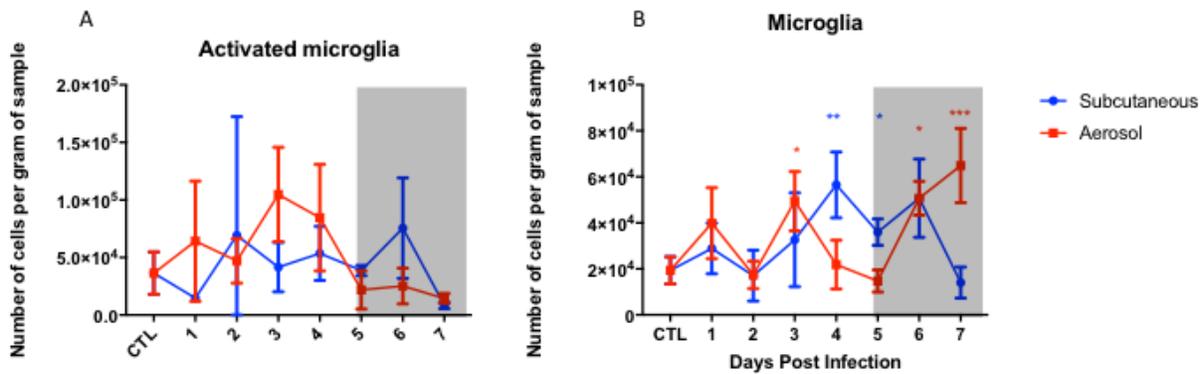
Figure 21. Activated and resting microglia phenotype in brain as a percentage of either CD45^{high} or CD45^{medium}.
Data determined through flow cytometry for both SC and AERO infected rats. Gating shown in figure 19. **A)** Activated microglia phenotype: CD45^{high}, Iba-1+, CD68+, CD11b+, CD163- and RP-1-. **B)** resting microglia phenotype CD45^{medium}, Iba-1+, CD68+, CD11b+, CD163- and RP-1-.
$P < 0.05 = *$, $P < 0.01$ **, $P < 0.001$ ***, $P < 0.0001$ ****

To confirm previous finding that His-48$^+$ RP-1$^+$ CD11b^{high} cells are neutrophils (Fig. 6), we analyzed the co-expressionlooked at coexpression of RP-1, CD68, and CD163 (Figure 2222 A-D). Using this new strategy, the majority of the RP-1$^+$, CD11b^{high} events also expressed CD68$^+$,

39

pan macrophage marker, but did not express CD163^{+} (Figure 2222 C-D). This finding suggests that CD68^{+} may not be exclusive to macrophages. This may make sense, as CD68 is a marker for lysosomal function and neutrophils can perform lysosomal function. Therefore, we incorporated CD68^{+} events into the gating strategy, but excluded CD163^{+} and Iba-1^{+} as exclusive macrophage markers (Figure 23 A-C). Overall, the new gating strategy did not change our previous findings, (Figure 7), and demonstrated that phenotypic neutrophils are a large proportion of events seen in AERO-infected, starting 5dpi, and not significant in SC-infection (Figure 24).
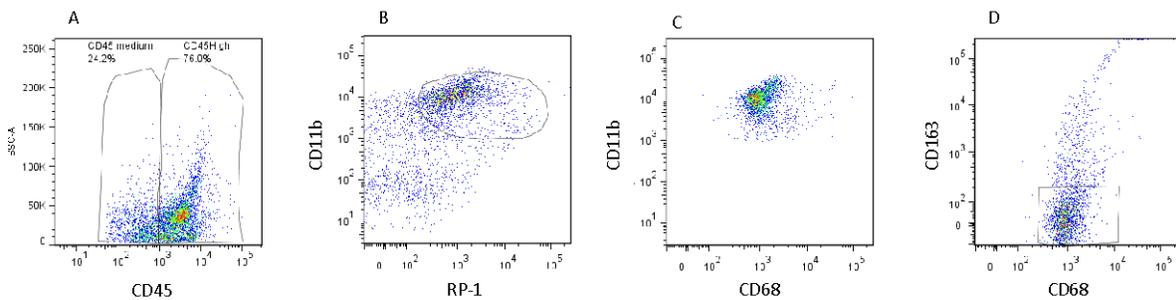
Figure 22. Phenotyping neutrophils using new panel for conformation of previous gating strategy.
A) CD45 positive events broken down into medium and high expression. **B)** Gated on CD45^{high} expression to show CD11b expression and RP-1 expression. **C)** Gated on RP-1+ and CD11b+ population to show CD68 expression and CD11b^{high}. **D)** Gated on CD68+ CD11b+ expression to show CD163+ and CD68+.
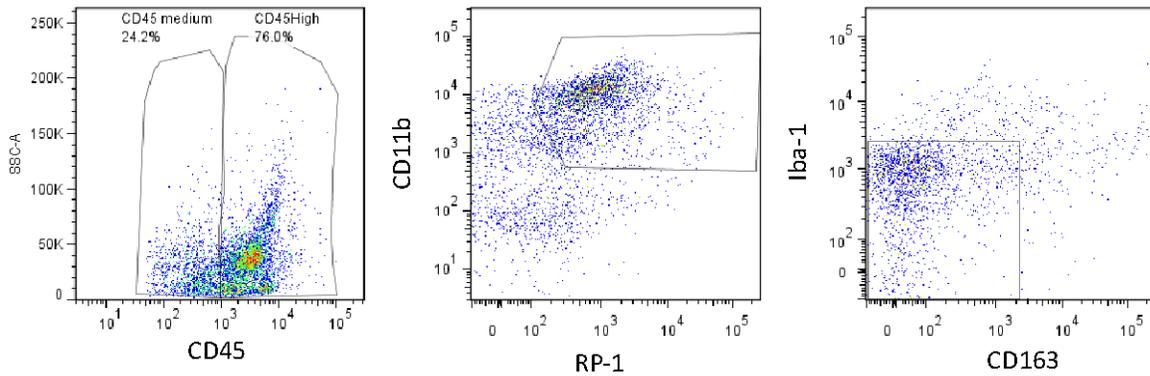
Figure 23. Neutrophil identification gating strategy in RVFV infected rat brain.

A) CD45 positive events broken down into medium and high expression. **B)** Gated on CD45^{high} expression to show CD11b expression and RP-1 expression. **C)** Gated on RP-1+ and CD11b+ population to show Iba-1- and CD163-.
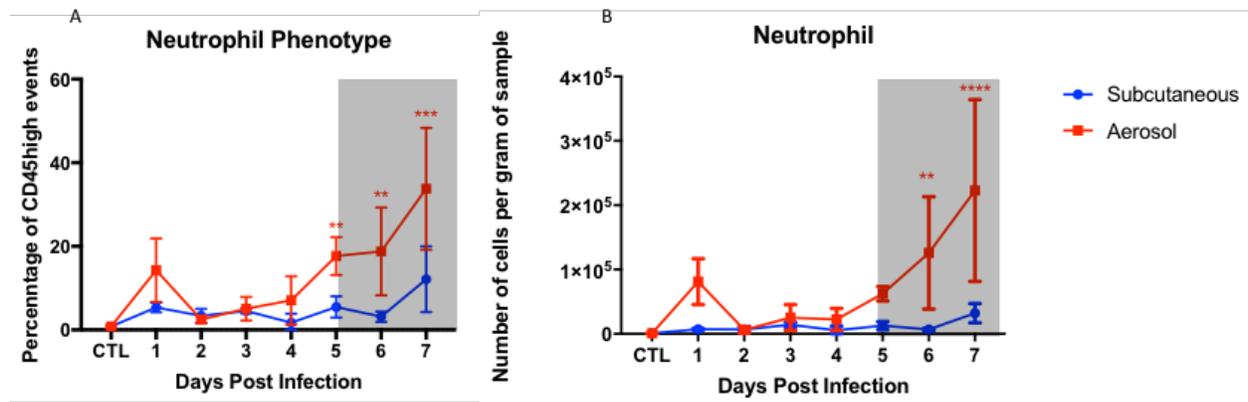
Figure 24. Neutrophil phenotype in brain as a percentage of CD45^{high}.

Data determined through flow cytometry for both SC and AERO infected rats. Gating shown in Figure 22. Phenotyped as RP-1+, CD11b+, CD68+, Iba-1-, CD163-. $P < 0.05$ = *, $P < 0.01$ **, $P < 0.001$ ***, $P < 0.0001$ ****

Finally, we tried to confirmed neutrophil phenotype of CD11b +, RP-1 + with Calprotectin, a neutrophil marker, (Figure 2525 A-D). It is plausible that RP-1 may have some off target effects, causing it to bind macrophages. To control for this, we excluded CD163^{+} events in the gating strategy (Figure 24 D). However, this still did not reflect our findings in Fig. 7 and 24 (Figure 26).

41

Both infection routes seem to mirror each other with respect to increases and decreases of CD45^{high} events. Since these were gated on RP-1 and CD11b, they are likely neutrophils but calprotectin could be identifying a subset of the neutrophils.
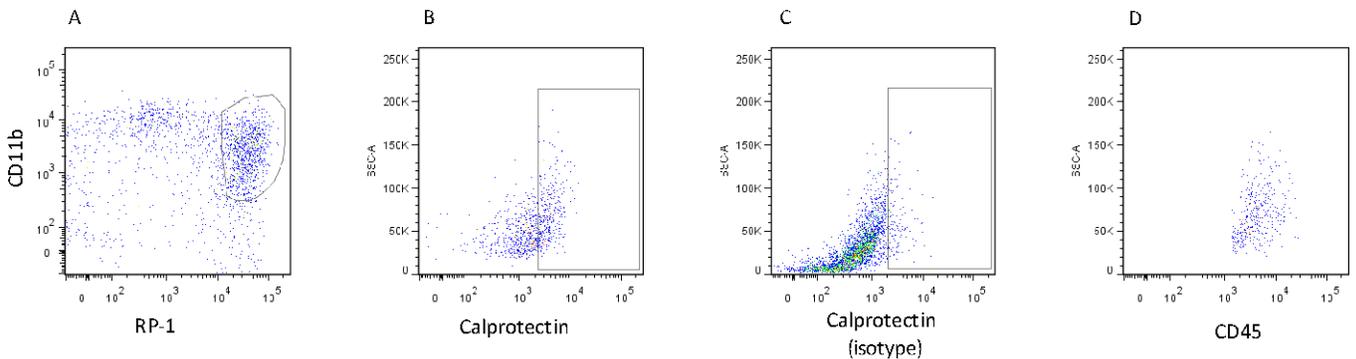
Figure 25. Neutrophil identification gating strategy using Calprotectin as confirmation.

All data gated on Vital brain gate, singlet inclusion and CD45high expression. **A)** Gated on CD45^{high} events to show RP-1 and CD11b expression. **B)** Gated on CD11b and RP-1 positive events to show calprotectin expression. **C)** Calprotectin isotype to confirm gating strategy gating shown in B. **D)** Gated on calprotectin positive to show CD45 expression and side scatter distribution.
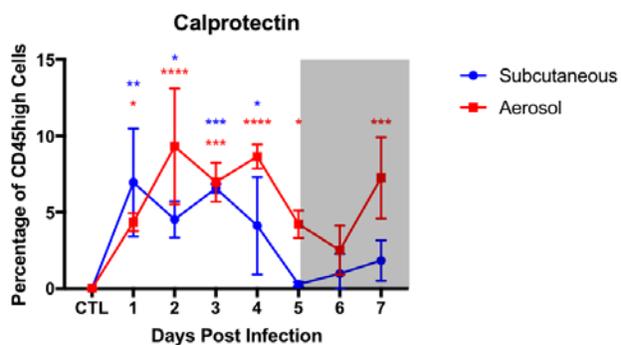
Figure 26. Neutrophils over time based on calprotectin confirmation.

$P < 0.05$ = *, $P < 0.01$ **, $P < 0.001$ ***, $P < 0.0001$ ****

4.2   SPECIFIC AIM 2

4.2.1   Specific Aim 2A

For all brain samples in Aim 1, we have matched blood samples that we used to understand changes in cell phenotypes in the periphery that could correlated with viral encephalitis. As with the brain, there was a general gating strategy performed to initially analyze all whole blood samples from each infection route (Figure 2727 A-C). Since there were clearly defined side scatter populations, these was used as an initial gate for lymphocyte, macrophage/monocyte, and neutrophil populations (Figure 2727 D).
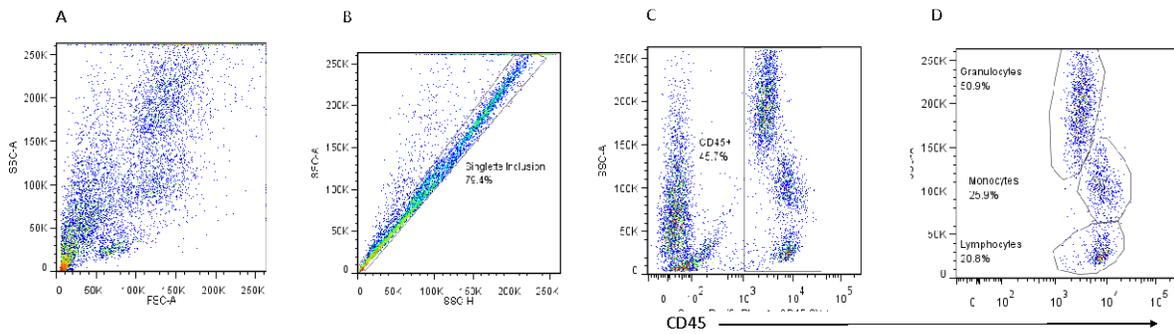
Figure 27. Flow cytometry gating strategy for leukocytes in RVFV infected Lewis rat whole blood.

These gates represent the base gates for all other strategies shown in this aim. **A)** This is ungated events shown by side scatter and granularity. **B)** Singlet inclusion to exclude any confounding cells. **C)** CD45+ gate to identify leukocytes. **D)** Leukocytes gated based on side scatter to reveal granulocytes, monocytes, and lymphocytes based on descending side scatter, respectively.

There was a clear indication of systemic response in the AERO-infected rats, while the SC-infected rats demonstrated fewer CD45$^+$ events (Figure 2828 A-C). Moreover, there was a

significant increase in cells of granulocytic side scatter on 3, 4, and 6 dpi for AERO-infected rats, while there was no increase for SC-infected animals (Figure 29 A), and this confirms our previously published data showing granulocytosis in the blood as measured by standard CBC (43). Monocytes (based on light scatter properties) were not observed to change statistically significantly in either infection route at any time that was studied (Figure 29 B). However, lymphocytes were significantly decreased in AERO-infected rats starting on 3dpi, while there was no difference from SC-infected rats compared to the control (Figure 29 C). This could be due to a proportional increase in AERO-infected, as granulocytes based on side scatter are increasing at the same time (Figure 29 A and C).
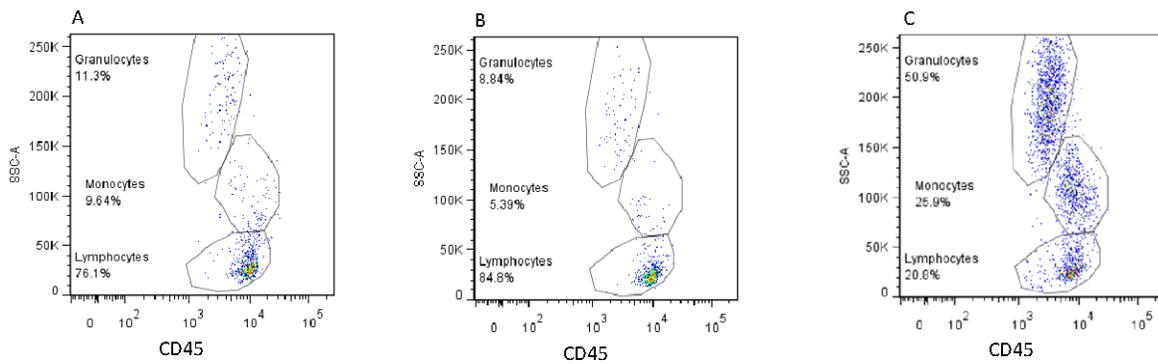
Figure 28. Breakdown of leukocytes based on side scatter across various infection routes at 6dpi for RVFV infected rat whole blood.

All base gating is shown in Figure 26B-D. **A)** Uninfected control **B)** SC exposed 6dpi **C)** AERO exposed 6dpi.

44
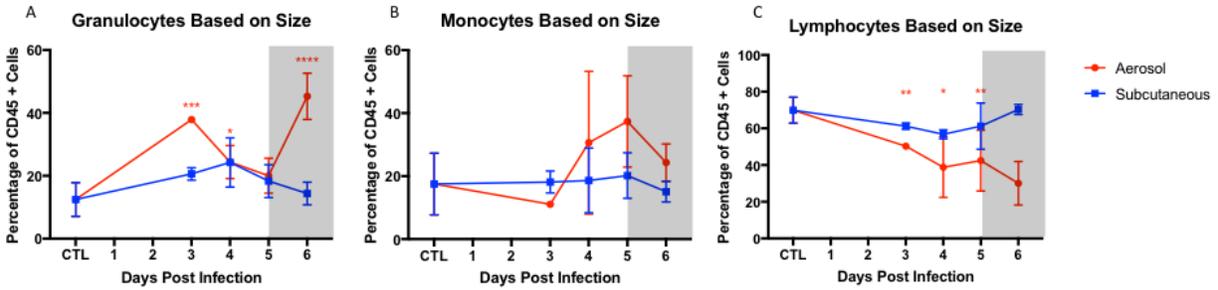
Figure 29. Blood leukocytes side scatter and CD45 expression as a percentage of CD45+ gate.

Data determined through flow cytometry for both SC and AERO infected rats. Gating shown in Figure 22. **A)** Granulocytes based on side scatter and CD45 expression. **B)** Monocytes based on side scatter and CD45 expression. **C)** Lymphocytes based on side scatter and CD45 expression. $P < 0.05 = *$, $P < 0.01 **$, $P < 0.001 ***$, $P < 0.0001 ****$

For the identification of peripheral neutrophils, the same markers were used as in the brain (Figure 30 A-C). Here, almost all events that were this side scatter were His-48^{+}, Rp-1^{+}, and CD11b^{+}. There was no difference in neutrophils in SC-infected animals over time, but there was an increase within the AERO-infected rats on 3, 4 and 6dpi (Figure 31). The initial increase in phenotypic neutrophils in the blood may give rise to the neutrophils seen in the brain on 5dpi, shown previously for AERO-infected rats (Fig. 7 and Fig. 24).
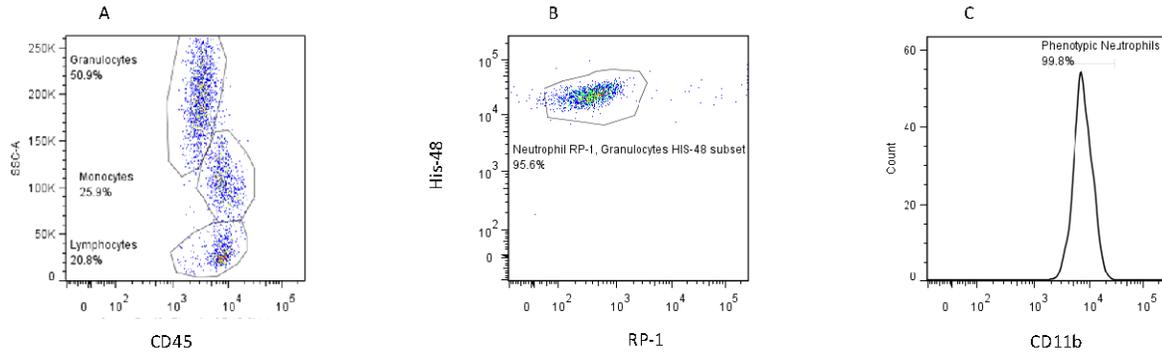
Figure 30. Neutrophil gating strategy for RVFV infected rat whole blood.

All base gating is shown in Figure 26. **A)** Shows CD45+ leukocytes distinguished by side scatter. **B)** Gated on granulocyte side scatterd population to show expression of His-48 and RP-1. **C)** Gated on His-48+, RP-1+ positive events to show CD11b expression.
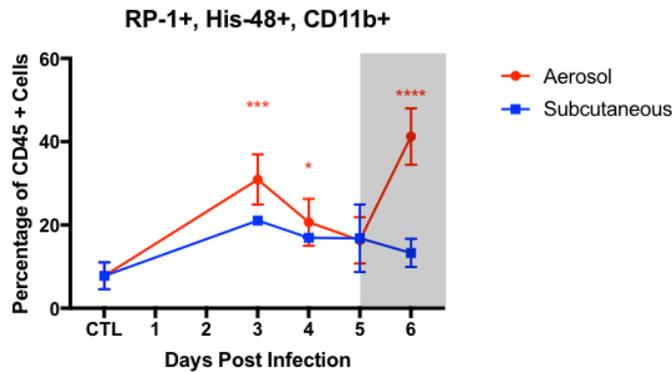
Figure 31. Neutrophil phenotype expression in whole blood as percentage of CD45+ events

Data determined through flow cytometry for both SC and AERO infected rats. Gating shown in Figure 29. Neutrophils in whole blood were phenotyped as RP-1+, His-48+, and CD11b+. $P < 0.05$ *, $P < 0.01$ **, $P < 0.001$ ***, $P < 0.0001$ ****

Next we turned our attention to macrophages/monocytes. While there was no difference in the number of macrophages based light scatter properties and CD45 expression,, there was a difference in their expression of the phenotypic markers CD163 and CD68. These cells were classified as M2 (CD163+ CD68-), M1 (CD68+ CD163-), or as double positive (CD163+ and

46

CD68+) (Figure 3232 A-B). This classification was based on a similar study that demonstrated the phenotypes of these cells in tumors (47). M1 macrophages were seen in proportional increases in only AERO-infected 5dpi (Figure 33 A). This finding is particularly interesting because M1 macrophages are classical macrophages, associated with inflammation (47). M2 macrophages, generally thought of as immune suppressive, decreased for AERO-infected when compared with control for each time point studied. The high levels of this cell type make sense for the control, as a suppressive phenotype should be expected for a non-disease/infected state. SC-infected rats also saw a significant decrease in M2, but later, starting on 5dpi (Figure 3333 C). The retention of high M2 cells could have implications for viral control in the periphery. Double positive macrophages were seen at higher than control levels for all days of AERO-infected but only for 3 and 4dpi for SC-infected, (Figure 33 B). Therefore, it can be inferred that while there is not a significant change in the number of overall macrophages, there are phenotypic differences occurring during the course of each infection that could have an impact on the inflammatory response to the viral insult.

Figure 32. Blood monocyte gating strategy in RVFV infected rat whole blood.

All base gating is shown in Figure 26 **A)** Shows CD45+ leukocytes distinguished by side scatter. **B)** CD68 and CD163 expression on cells in the monocyte gate from A).

47
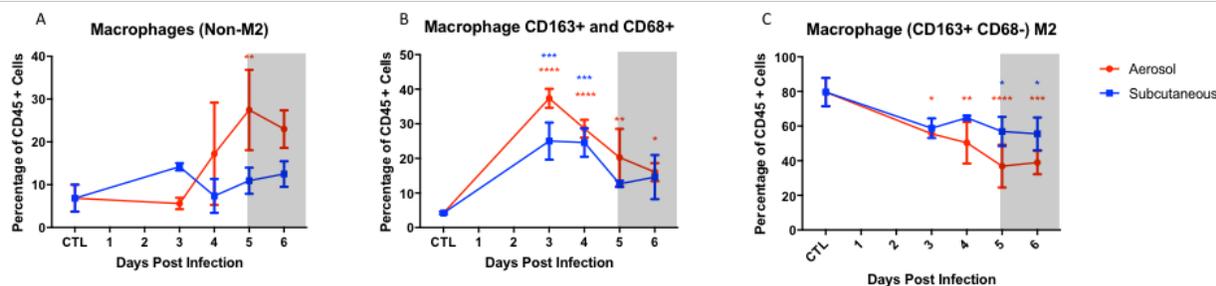
Figure 33. Monocyte/Macrophage marker expression in whole blood as a percentage of CD45+.

Data determined through flow cytometry for both SC and AERO infected rats. Gating shown in Figure 31. **A)** non-M2 macrophages are those events that are CD68+ and CD163- **B)** Macrophages CD163+ and CD68+ **C)** M2 macrophages are those that are CD163+ and CD68-. $P < 0.05$ *, $P < 0.01$ **, $P < 0.001$ ***, $P < 0.0001$ ****

T lymphocytes were also phenotyped in whole blood, (Figure 3434 A-C). Overall, there was not much fluctuation with overall T cells as determined by $CD3^+$ as a percentage of lymphocyte side scatterd events (Figure 3535 A). Both CD4+ cells and CD8+ cells also did not change significantly during the course of infection for either infection route as a percentage of lymphocyte side scatterd events (Figure 3535 B-C). While overall there was a decrease of lymphocyte events for AERO-infected, it does not appear that T cell events change over time.

48
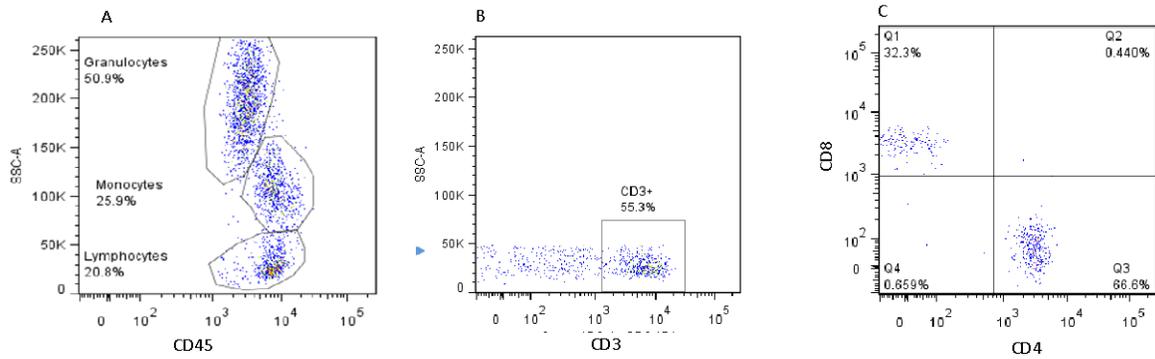
Figure 34. T Lymphocyte gating strategy in RVFV infected rat whole blood.

All base gating is shown in Figure 26 **A)** Shows CD45+ leukocytes distinguished by side scatter. **B)** CD3 expression on lymphocyte-gated cells. **C)** CD4+ and CD8+ expression on CD3+ lymphocytes.
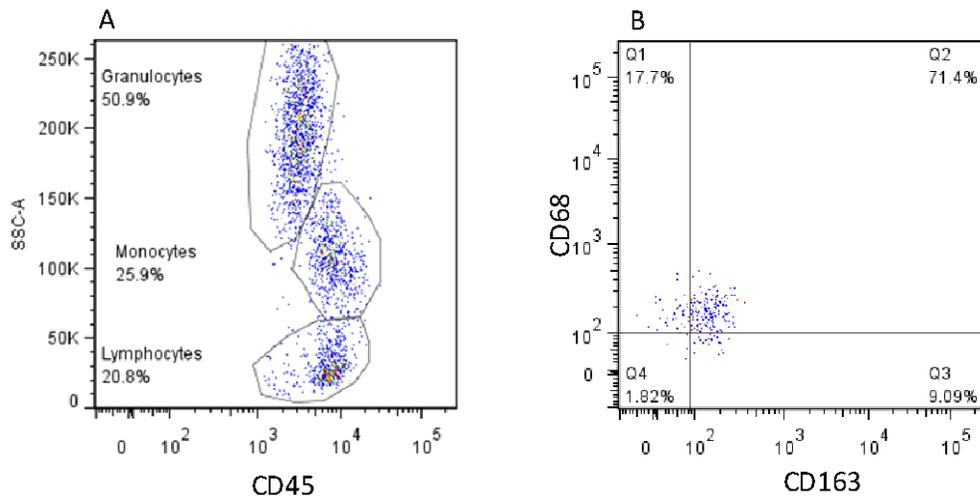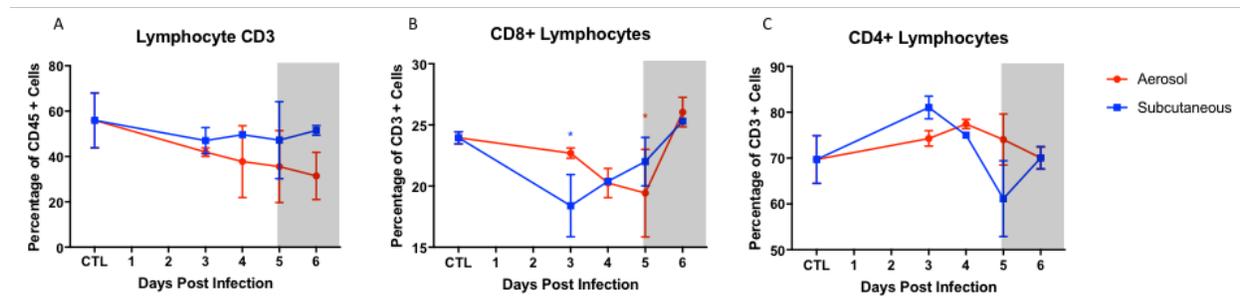

Figure 35. T lymphocyte marker expression in whole blood as a percentage of CD45+.

Data determined through flow cytometry for both SC and AERO infected rats. Gating shown in Figure 33. **A)** T lymphocytes phenotyped by CD3+. **B)** CD8+ lymphocytes phenotyped by CD3+ and CD8+. **C)** CD4+ lymphocytes phenotyped by CD3+ and CD4+. $P < 0.05$ = *, $P < 0.01$ **, $P < 0.001$ ***, $P < 0.0001$ ****

49

5.0   DISCUSSION

RVFV is an arbovirus that poses a safety threat from both natural or intentional spread (48). This virus has the capability to cause severe disease in humans and can potentially wipe out swaths of livestock in its wake. Moreover, outbreaks appear to be increasing in frequency and scope, with an outbreak ongoing every year, somewhere, for the last six years. Using immunocompetent Lewis rats, we were able to uniformly recapitulate the neurological disease through AERO exposure to RVFV (43). In doing so, we were able to study the leukocytes entering the CNS throughout the course of infection and compare the neurological disease created by lethal AERO exposure to the sub-lethal SC exposure route, which exhibit no apparent disease. Leukocyte infiltration to the CNS is consistent with other viruses that result in encephalitis, such as JEV and new world alphaviruses (49, 50). Additionally, human cases of RVFV-induced encephalitis have demonstrated increased leukocytes present in the cerebral spinal fluid and brain pathology, suggesting that infiltration may be a part of human clinical disease as well (51).

We observed a significant increase inf leukocyte density isolated from brains of AERO-infected rats, but not from brains of SC-infected rats. This is suggestive of immune cell infiltration to the CNS from the periphery of the AERO-infected rats, resulting in encephalitis. Alternatively, this could be the result of subsets of leukocytes already present in the CNS proliferating. This is unlikely to be the case, as previous experiments in our lab show that the reduced integrity of the BBB correlated with increased leukocytes, which seems to point more towards peripheral infiltration than expansion of already present leukocytes, though both may be happening at some level. For the $CD45^{high}$ and $CD45^{med}$ cells in each experiment, we saw differences based on whether we looked at proportions of cells within a given gate or absolute numbers, though both reflected

50

the same trends. This highlights an important drawback of doing this analysis through flow cytometry as it can make direct comparisons difficult between infection routes that result in more cells in the brain. Overall, we were able to suggest that AERO-infected did have more phenotypic leukocytes, both proportionally and in terms of cell counts, while both infection routes had more microglia than the control, just in terms of cell counts.

We sought to identify what cells constitute the $CD45^{high}$ population. Using histology, previous studies showed the appearance of neutrophils in the brain of rats dying from RVF encephalitis (43). Using His-48 (pan-granulocyte marker), RP-1 (neutrophil marker), and CD11b (integrin subunit), we found neutrophils in the CNS of AERO but not SC-infected rats. The increase in neutrophils occurred at 5 dpi, which is the start of the clinical window seen in the AERO-infected rats. For further confirmation of the neutrophil population, we conducted a subsequent study with additional markers. We gated on $CD11b^{high}$ and $RP-1^+$ within the $CD45^{high}$ gate. Gated on the double positive population, we gated on the macrophage markers CD68 and CD163. Almost all $RP-1^+$ $CD11b^+$ events were also $CD68^+$, much to our surprise. However, it is now understood that neutrophils can express CD68, as it is an indicator of lysosome activity (52). This is not a case of indiscriminate uptake of antibody, as the cells were neither positive for CD163 nor Iba-1, as demonstrated through gating. Therefore, the neutrophil phenotype appears to be $RP-1^+$, $CD11b^+$, and $CD68^+$. The results of this new gating, however, did not alter our previous findings of neutrophil infiltration as a percentage of the $CD45^{high}$ population. Therefore, $CD45^{high}$, $RP-1^+$, $CD11b^+$ is sufficient for phenotyping infiltrating neutrophils into the CNS and can be confirmed through these two experiments.

We also looked at the $RP-1^+$ $CD11b^+$ phenotype and co-expression with calprotectin. Calprotectin is typically found on neutrophils or weakly on macrophages, where it functions as a

heterodimer antibacterial/fungal protein through metal sequestration and can be released from its cytosolic form in the lumen of the gut (53). When the calprotectin+ population was investigated, it was determined that some, but not all CD11b$^+$, RP-1$^+$ cells also expressed calprotectin. This could be because calprotectin is not exclusive to neutrophils entering the CNS and can be expressed on monocytes (53). Additionally, it is possible that calprotectin is found on a subset of neutrophils in the gut and not infiltrating neutrophils in the brain. RP-1 is a marker that has been shown to identify both immature and mature neutrophils in blood (54). Calprotectin, alternatively, has been shown in human neonates to be present more present with immature neutrophils (55). This suggests that these calprotectin$^+$ events in rats, may be representative of immature neutrophils. Few studies have looked at calprotectin in the context of viral encephalitic disease, and more investigation is required to understand exactly what cells are expressing calprotectin in the event of viral encephalitis. The overall implications of calprotectin in the neutrophil population remain unclear.

While there is still insufficient evidence to ascertain if the pathologic neurological disease exhibited in AERO-infected rats is due to virus itself or immunological damage, the increase in neutrophils may suggest a potential etiology. Neutrophils are highly inflammatory cells, often producing damage in an attempt to limit viral spread without regard to tissue preservation(56). Neutrophils have also been implicated in the loss of BBB integrity after transmigration, through an MMP dependent pathway, and could be implicated in the dramatic increase in leukocytes (CD45^{high}) observed after their influx as seen in Japanese Encephalitis Virus (24, 49). Our data is also supported by a previous finding from our lab that Gro/KC, a rat neutrophil-attracting chemokine homologous to human CXCL1, was found to be elevated at 4 dpi in the serum of AERO-infected rats (43). High levels of serum Gro/KC the day prior to the influx of neutrophils

in the CNS may imply the recruitment and proliferation in the periphery and gives reason why peripheral neutrophils may be entering the CNS. Additional chemokines, such as MCP-1 were also found to be significantly elevated in the serum, and may contribute to this proposed means of leukocyte entry to the CNS. Overall, the presence of neutrophils, combined with previous pathological data seem to suggest that the immune response contributes to the overt disease state in the AERO-infected rats. Further research is needed to understand the implications of these findings. Neutrophil depletion studies could look at the neutrophils role in death from neurological disease in AERO. Using genetically modified rats that expressed a reporter protein in neutrophils would also be useful, as this could help explain infiltration of the neutrophil phenotype to the brain. Additional studies should be done to understand the effector function of neutrophils in the brain, as it is no clear what they are doing. A first look at this might include translational analysis of neutrophils, to determine what genes they are making into proteins for effector function.

Unlike the significant changes in neutrophils, macrophages did not appear to be a significant contributor to disease in AERO-infected rats. The lack of a true microglia specific marker has hampered our efforts as well as the field for some time. We used Iba-1, a potential microglia-specific marker to determine if microglia were upregulating CD45 upon activation, as suggested by our earlier gating strategy (57). Our new gating strategy (Aim 1b) determined that activated microglia were depleted, as we had previously shown. This makes sense, as CD45^{high} is also the gate where phenotypic neutrophils will be and if they are contributing more to the population of AERO-infected and expressing CD68 then we would expect less activated microglia phenotype as a proportion of CD45^{high}. This also furthers the suggestion that AERO-infection immune response is driven by neutrophils in the CNS, since they make up a large percentage of the CD45^{high} events. Conversely, SC-infected may be protected by an increased or retained

53

activated microglial population. Overall, CD45^{high} macrophage linage populations do not appear to fluctuate in response to RVFV AERO-infection in rats, likely because of neutrophil infiltration. Blood macrophages also did not change. SC-infected rats also do not exhibit a large uptick in these phenotypes, proposing some other cell type could be involved in the lack of apparent neurological disease.

Phenotypic microglia, like the potentially infiltrating macrophages, microglia did not seem change dramatically to compared to control levels. In the two experiments we demonstrated that SC-infected rats have an early increase from control levels, while AERO-infected seemed to have late phenotypic microglia. This finding could implicate a rapid innate response to RVFV in the lack of neurological disease in SC-infected, as virus has been found in the CNS and surrounding tissue as early as 2dpi (58). Microglia are tightly regulated in terms of immune function, so if they are able to control the infection early, it may reduce later responses when viral loads cause a cytokine storm as seen in AERO-infected rats (43).This is the case in some Flaviviruses that cause encephalitis, such as dengue. Dengue infection has shown to be slowed down by the early activation of microglia (59). Taken together, the role of microglia in the neurological disease may be an important one and are the first responders to viral insult, but are not clearly tracked through infection. Microglia depleted from the CD45^{med} phenotype do not appear to be upregulating CD45 and entering the activated microglia phenotype. While it is only speculative, it may be that these microglia are becoming infected themselves and dying before ever becoming activated. Alternatively, they may be dying after brief functional activation. This would fit with our data, as microglia are not appearing elsewhere. Having said this, our study looks at the proportions of leukocytes in the brain and additional work is required before insight into the role of microglia in RVFV infection can be fully understood.

Lymphocyte infiltration was also identified in previous studies which suggested it may be important in RFVF encephalitis (58). One such study used intranasal and SC-infection of a mouse model, where it was demonstrated that SC-infected mice mounted a stronger T cell response and died later during infection compared to the intranasal-infected mice (58). This also correlated with increased viral loads in the brain of intranasal-infected mice compared to the SC-infected mice, suggesting the T cell response may control viral replication in the brain (58). Here we found the proportion of $CD3^+$ cells was significantly higher for SC-infected rats on 6dpi, while AERO-infected rats had decreased CD3+ cells in the CNS compared to controls as early as 5dpi. A word of caution should be used here, as the drop observed is based on the percentage of total cells, not an actual count. The decrease could be due to increased neutrophils in AERO–infected rats. Further analysis of T lymphocytes revealed that there were $CD4^+$ T cell responses in the SC on day 6dpi while AERO was significantly lower on 6dpi. Additionally, SC has a transient decrease in proportion of $CD8^+$ cells on 3dpi, but then recovers to near control levels during the clinical window. This mirrors what was previously seen in the periphery by CBC and presence of RANTES, a lymphocyte chemokine, where there is a biphasic peak showing lymphocytes decreasing on 3dpi (43). It is unclear what implications this could have on the course of infection. However, the large T cell response for the SC-infected might be expected, given the location of initial infection. By infection taking place through the skin, the virus encounters far more antigen presentation cells, such as dendritic cells, that are absent in the CNS, where AERO infection is thought to take root. Therefore, more naïve T cells can be activated, more effectively in the SC-infected than the AERO-infected, controlling the viral replication and reducing the apparent pathogenesis. Taken together, this suggests a strong component of the SC response is mediated by T cells, specifically CD4, while T cell appears to be lacking in the AERO-infected rats.

Altogether, these data suggest two important points for RVFV infection and the resulting neurological disease. The first important point is the infiltration of neutrophils in AERO-infected on 5dpi and later while there is no significant neutrophil infiltration of the brain in SC-infected. This infiltration is the starkest difference between these infection routes and is confirmed by histology, cytokines present in both serum and brain, the same phenotypic neutrophils increasing in the serum a day before infiltration, and BBB breakdown. Our lab has recently learned that the BBB breaks down during RVFV AERO-infection through an MMP-9 independent manner. As previously mentioned, neutrophils produced MMP-9 during transmigration in other viral encephalitis infections and reduce vascular integrity of the BBB. The subsequent reduction in vascular integrity of this barrier can then allow unchecked immune infiltrate into the CNS of the AERO-infected. Therefore, these data put together suggest a mechanism for BBB, why AERO-infected may see larger amounts of immune infiltrate than SC-infected, and potentially, why neurological disease occurs in AERO- but not SC-infected. The neutrophil dominated disease has been seen in other arboviruses such as Japanese Encephalitis Virus and West Nile Virus (12, 60). Neutrophils remain understudied in terms of virology and specifically their role in viral induced encephalitis and, as demonstrated through our work, likely play an important part in the role of immune response to neurological disease.

The second important point is that SC-infected rats show an increase in CD4$^+$ T cells, while AERO-infected does not significantly differ from controls. The larger number of CD4$^+$ T cells in the SC-infection make sense, since the infection initial takes place were a large number of dendritic cells are present and can stimulate naïve T cells. Alternatively, the AERO-infected rats may have to rely on microglia, a poor antigen presenter, for T cell activation and thus elicit a more innate response to control infection. Several studies have demonstrated T cell activation resulting in

56

leukocytes that lack effector function from chronic infection or poor antigen presentation (61, 62). In mouse models of RVFV, this same mechanism of CD4+ T cells lacking effector function has been suggested for the cause of death in intranasal infection but not subcutaneous injection of RVFV (58, 63). Therefore, this finding builds on an existing field of research that suggests an important role for CD4+ cells for SC-infection but not for AERO-infection. Overall, AERO-infection appears to be dominated by neutrophil infiltration into the brain while SC-infection is dominated by CD4 cells, despite viral antigen in both brains (Figure 36).
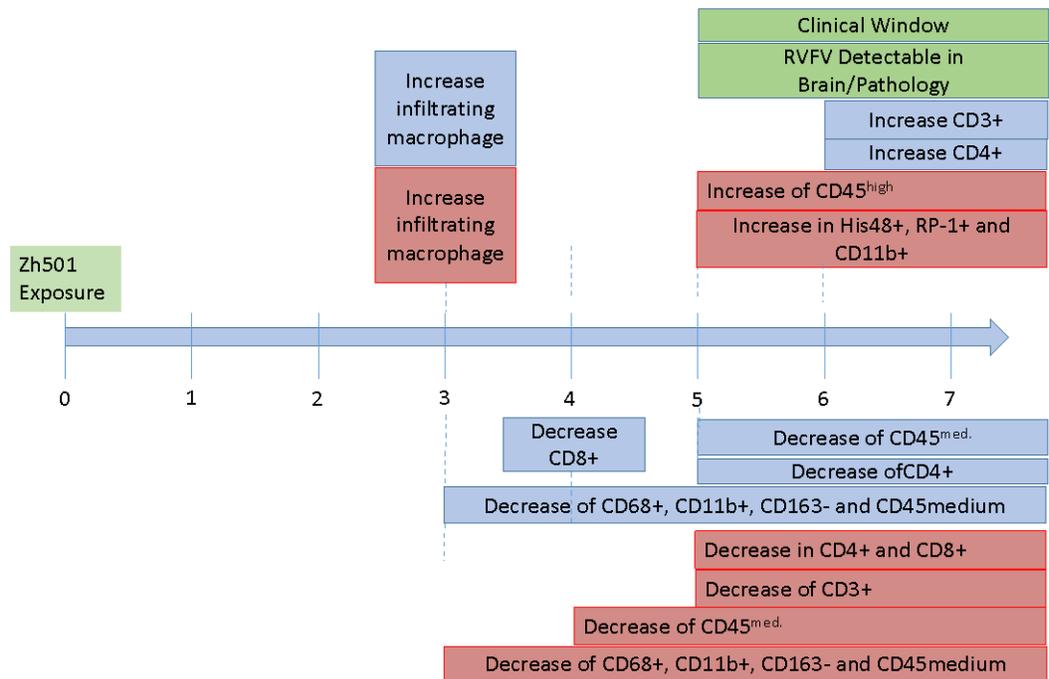
Figure 36. Summary of phenotypic changes in CNS from 1-7dpi from exposures.

BIBLIOGRAPHY

1.   **Silva MT.** 2013. Viral encephalitis. Arq Neuropsiquiatr **71:**703-709.
2.   **Griffin DE.** 2003. Immune responses to RNA-virus infections of the CNS. Nat Rev Immunol **3:**493-502.
3.   **Harling-Berg CJ, Park TJ, Knopf PM.** 1999. Role of the cervical lymphatics in the Th2-type hierarchy of CNS immune regulation. J Neuroimmunol **101:**111-127.
4.   **Cebrian C, Loike JD, Sulzer D.** 2014. Neuronal MHC-I expression and its implications in synaptic function, axonal regeneration and Parkinson's and other brain diseases. Front Neuroanat **8:**114.
5.   **Medana I, Li Z, Flugel A, Tschopp J, Wekerle H, Neumann H.** 2001. Fas ligand (CD95L) protects neurons against perforin-mediated T lymphocyte cytotoxicity. J Immunol **167:**674-681.
6.   **Cabezas R, Avila M, Gonzalez J, El-Bacha RS, Baez E, Garcia-Segura LM, Jurado Coronel JC, Capani F, Cardona-Gomez GP, Barreto GE.** 2014. Astrocytic modulation of blood brain barrier: perspectives on Parkinson's disease. Front Cell Neurosci **8:**211.
7.   **McGavern DB, Kang SS.** 2011. Illuminating viral infections in the nervous system. Nat Rev Immunol **11:**318-329.
8.   **Casiraghi C, Dorovini-Zis K, Horwitz MS.** 2011. Epstein-Barr virus infection of human brain microvessel endothelial cells: a novel role in multiple sclerosis. J Neuroimmunol **230:**173-177.
9.   **Clay CC, Rodrigues DS, Ho YS, Fallert BA, Janatpour K, Reinhart TA, Esser U.** 2007. Neuroinvasion of fluorescein-positive monocytes in acute simian immunodeficiency virus infection. J Virol **81:**12040-12048.
10. **Curanovic D, Enquist L.** 2009. Directional transneuronal spread of alpha-herpesvirus infection. Future Virol **4:**591.
11. **Shigemori Y, Katayama Y, Mori T, Maeda T, Kawamata T.** 2006. Matrix metalloproteinase-9 is associated with blood-brain barrier opening and brain edema formation after cortical contusion in rats. Acta Neurochir Suppl **96:**130-133.
12. **Tung WH, Tsai HW, Lee IT, Hsieh HL, Chen WJ, Chen YL, Yang CM.** 2010. Japanese encephalitis virus induces matrix metalloproteinase-9 in rat brain astrocytes via NF-kappaB signalling dependent on MAPKs and reactive oxygen species. Br J Pharmacol **161:**1566-1583.
13. **Delhaye S, Paul S, Blakqori G, Minet M, Weber F, Staeheli P, Michiels T.** 2006. Neurons produce type I interferon during viral encephalitis. Proc Natl Acad Sci U S A **103:**7835-7840.
14. **Mao X, Phanavanh B, Hamdan H, Moerman-Herzog AM, Barger SW.** 2016. NFkappaB-inducing kinase inhibits NFkappaB activity specifically in neurons of the CNS. J Neurochem **137:**154-163.
15. **Terasaki K, Ramirez SI, Makino S.** 2016. Mechanistic Insight into the Host Transcription Inhibition Function of Rift Valley Fever Virus NSs and Its Importance in Virulence. PLoS Negl Trop Dis **10:**e0005047.

16. **Sironi M, Forni D, Clerici M, Cagliani R.** 2016. Nonstructural Proteins Are Preferential Positive Selection Targets in Zika Virus and Related Flaviviruses. PLoS Negl Trop Dis **10:**e0004978.

17. **Lawson LJ, Perry VH, Gordon S.** 1992. Turnover of resident microglia in the normal adult mouse brain. Neuroscience **48:**405-415.

18. **Hayes GM, Woodroofe MN, Cuzner ML.** 1987. Microglia are the major cell type expressing MHC class II in human white matter. J Neurol Sci **80:**25-37.

19. **Ludowyk PA, Willenborg DO, Parish CR.** 1992. Selective localisation of neuro-specific T lymphocytes in the central nervous system. J Neuroimmunol **37:**237-250.

20. **Priller J, Flugel A, Wehner T, Boentert M, Haas CA, Prinz M, Fernandez-Klett F, Prass K, Bechmann I, de Boer BA, Frotscher M, Kreutzberg GW, Persons DA, Dirnagl U.** 2001. Targeting gene-modified hematopoietic cells to the central nervous system: use of green fluorescent protein uncovers microglial engraftment. Nat Med **7:**1356-1361.

21. **Tanaka R, Komine-Kobayashi M, Mochizuki H, Yamada M, Furuya T, Migita M, Shimada T, Mizuno Y, Urabe T.** 2003. Migration of enhanced green fluorescent protein expressing bone marrow-derived microglia/macrophage into the mouse brain following permanent focal ischemia. Neuroscience **117:**531-539.

22. **Varvel NH, Grathwohl SA, Baumann F, Liebig C, Bosch A, Brawek B, Thal DR, Charo IF, Heppner FL, Aguzzi A, Garaschuk O, Ransohoff RM, Jucker M.** 2012. Microglial repopulation model reveals a robust homeostatic process for replacing CNS myeloid cells. Proc Natl Acad Sci U S A **109:**18150-18155.

23. **Jeong HK, Ji K, Min K, Joe EH.** 2013. Brain inflammation and microglia: facts and misconceptions. Exp Neurobiol **22:**59-67.

24. **Zhou J, Stohlman SA, Hinton DR, Marten NW.** 2003. Neutrophils promote mononuclear cell infiltration during viral-induced encephalitis. J Immunol **170:**3331-3336.

25. **Subak-Sharpe I, Dyson H, Fazakerley J.** 1993. In vivo depletion of CD8+ T cells prevents lesions of demyelination in Semliki Forest virus infection. J Virol **67:**7629-7633.

26. **Pepin M, Bouloy M, Bird BH, Kemp A, Paweska J.** 2010. Rift Valley fever virus(Bunyaviridae: Phlebovirus): an update on pathogenesis, molecular epidemiology, vectors, diagnostics and prevention. Vet Res **41:**61.

27. **Zeller HG, Fontenille D, Traore-Lamizana M, Thiongane Y, Digoutte JP.** 1997. Enzootic activity of Rift Valley fever virus in Senegal. Am J Trop Med Hyg **56:**265-272.

28. **Faye O, Freire CC, Iamarino A, Faye O, de Oliveira JV, Diallo M, Zanotto PM, Sall AA.** 2014. Molecular evolution of Zika virus during its emergence in the 20(th) century. PLoS Negl Trop Dis **8:**e2636.

29. **Gargan TP, 2nd, Jupp PG, Novak RJ.** 1988. Panveld oviposition sites of floodwater Aedes mosquitoes and attempts to detect transovarial transmission of Rift Valley fever virus in South Africa. Med Vet Entomol **2:**231-236.

30. **Davies FG, Linthicum KJ, James AD.** 1985. Rainfall and epizootic Rift Valley fever. Bull World Health Organ **63:**941-943.

31. **LaBeaud AD, Pfeil S, Muiruri S, Dahir S, Sutherland LJ, Traylor Z, Gildengorin G, Muchiri EM, Morrill J, Peters CJ, Hise AG, Kazura JW, King CH.** 2015. Factors associated with severe human Rift Valley fever in Sangailu, Garissa County, Kenya. PLoS Negl Trop Dis **9:**e0003548.

32. **Baudin M, Jumaa AM, Jomma HJ, Karsany MS, Bucht G, Naslund J, Ahlm C, Evander M, Mohamed N.** 2016. Association of Rift Valley fever virus infection with miscarriage in Sudanese women: a cross-sectional study. Lancet Glob Health **4:**e864-e871.

33. **Balkhy HH, Memish ZA.** 2003. Rift Valley fever: an uninvited zoonosis in the Arabian peninsula. Int J Antimicrob Agents **21:**153-157.

34. **Services. DoHaH.** 2005. Possession, Use, and Transfer of Select
Agents and Toxins; Final Rule. Federal Register **70**.

35. **de Boer SM, Kortekaas J, de Haan CA, Rottier PJ, Moormann RJ, Bosch BJ.** 2012. Heparan sulfate facilitates Rift Valley fever virus entry into the cell. J Virol **86:**13767-13771.

36. **Zamoto-Niikura A, Terasaki K, Ikegami T, Peters CJ, Makino S.** 2009. Rift valley fever virus L protein forms a biologically active oligomer. J Virol **83:**12779-12789.

37. **Billecocq A, Spiegel M, Vialat P, Kohl A, Weber F, Bouloy M, Haller O.** 2004. NSs protein of Rift Valley fever virus blocks interferon production by inhibiting host gene transcription. J Virol **78:**9798-9806.

38. **Le May N, Mansuroglu Z, Leger P, Josse T, Blot G, Billecocq A, Flick R, Jacob Y, Bonnefoy E, Bouloy M.** 2008. A SAP30 complex inhibits IFN-beta expression in Rift Valley fever virus infected cells. PLoS Pathog **4:**e13.

39. **Yamaoka S, Ebihara H.** 2016. The two faces of Rift Valley fever virus virulence factor NSs: The development of a vaccine and the elucidation of pathogenesis. Virulence doi:10.1080/21505594.2016.1213938**:**1-4.

40. **Won S, Ikegami T, Peters CJ, Makino S.** 2007. NSm protein of Rift Valley fever virus suppresses virus-induced apoptosis. J Virol **81:**13335-13345.

41. **Kreher F, Tamietti C, Gommet C, Guillemot L, Ermonval M, Failloux AB, Panthier JJ, Bouloy M, Flamand M.** 2014. The Rift Valley fever accessory proteins NSm and P78/NSm-GN are distinct determinants of virus propagation in vertebrate and invertebrate hosts. Emerg Microbes Infect **3:**e71.

42. **Bales JM, Powell DS, Bethel LM, Reed DS, Hartman AL.** 2012. Choice of inbred rat strain impacts lethality and disease course after respiratory infection with Rift Valley Fever Virus. Front Cell Infect Microbiol **2:**105.

43. **Caroline AL, Kujawa MR, Oury TD, Reed DS, Hartman AL.** 2015. Inflammatory Biomarkers Associated with Lethal Rift Valley Fever Encephalitis in the Lewis Rat Model. Front Microbiol **6:**1509.

44. **Peters CJ, Slone TW.** 1982. Inbred rat strains mimic the disparate human response to Rift Valley fever virus infection. J Med Virol **10:**45-54.

45. **Moller K, Stahl T, Boltze J, Wagner DC.** 2012. Isolation of inflammatory cells from rat brain tissue after stroke. Exp Transl Stroke Med **4:**20.

46. **Walker DG, Lue LF.** 2015. Immune phenotypes of microglia in human neurodegenerative disease: challenges to detecting microglial polarization in human brains. Alzheimers Res Ther **7:**56.

47. **Harris JA, Jain S, Ren Q, Zarineh A, Liu C, Ibrahim S.** 2012. CD163 versus CD68 in tumor associated macrophages of classical Hodgkin lymphoma. Diagn Pathol **7:**12.

48. **Metras R, Baguelin M, Edmunds WJ, Thompson PN, Kemp A, Pfeiffer DU, Collins LM, White RG.** 2013. Transmission potential of Rift Valley fever virus over the course of the 2010 epidemic in South Africa. Emerg Infect Dis **19:**916-924.

49. **Li F, Wang Y, Yu L, Cao S, Wang K, Yuan J, Wang C, Wang K, Cui M, Fu ZF.** 2015. Viral Infection of the Central Nervous System and Neuroinflammation Precede Blood-Brain Barrier Disruption during Japanese Encephalitis Virus Infection. J Virol **89:**5602-5614.

50. **Charles PC, Trgovcich J, Davis NL, Johnston RE.** 2001. Immunopathogenesis and immune modulation of Venezuelan equine encephalitis virus-induced disease in the mouse. Virology **284:**190-202.

51. **Alrajhi AA, Al-Semari A, Al-Watban J.** 2004. Rift Valley fever encephalitis. Emerg Infect Dis **10:**554-555.

52. **Amanzada A, Malik IA, Blaschke M, Khan S, Rahman H, Ramadori G, Moriconi F.** 2013. Identification of CD68(+) neutrophil granulocytes in in vitro model of acute inflammation and inflammatory bowel disease. Int J Clin Exp Pathol **6:**561-570.

53. **Suryono, Kido J, Hayashi N, Kataoka M, Shinohara Y, Nagata T.** 2006. Norepinephrine stimulates calprotectin expression in human monocytic cells. J Periodontal Res **41:**159-164.

54. **Skrajnar S, Anzur Lasnik M, Bedina Zavec A.** 2009. A flow cytometric method for determination of the blood neutrophil fraction in rats. J Am Assoc Lab Anim Sci **48:**152-156.

55. **MacQueen BC, Christensen RD, Yost CC, Lambert DK, Baer VL, Sheffield MJ, Gordon PV, Cody MJ, Gerday E, Schlaberg R, Lowe J, Shepherd JG.** 2016. Elevated fecal calprotectin levels during necrotizing enterocolitis are associated with activated neutrophils extruding neutrophil extracellular traps. J Perinatol **36:**862-869.

56. **Tang FS, Van Ly D, Spann K, Reading PC, Burgess JK, Hartl D, Baines KJ, Oliver BG.** 2016. Differential neutrophil activation in viral infections: Enhanced TLR-7/8-mediated CXCL8 release in asthma. Respirology **21:**172-179.

57. **Korzhevskiy DE, Kirik OV.** 2015. [Cerebral Microglia and Microglial Markers]. Morfologiia **147:**37-44.

58. **Dodd KA, McElroy AK, Jones TL, Zaki SR, Nichol ST, Spiropoulou CF.** 2014. Rift valley Fever virus encephalitis is associated with an ineffective systemic immune response and activated T cell infiltration into the CNS in an immunocompetent mouse model. PLoS Negl Trop Dis **8:**e2874.

59. **Tsai TT, Chen CL, Lin YS, Chang CP, Tsai CC, Cheng YL, Huang CC, Ho CJ, Lee YC, Lin LT, Jhan MK, Lin CF.** 2016. Microglia retard dengue virus-induced acute viral encephalitis. Sci Rep **6:**27670.

60. **Bai F, Kong KF, Dai J, Qian F, Zhang L, Brown CR, Fikrig E, Montgomery RR.** 2010. A paradoxical role for neutrophils in the pathogenesis of West Nile virus. J Infect Dis **202:**1804-1812.

61. **Zajac AJ, Blattman JN, Murali-Krishna K, Sourdive DJ, Suresh M, Altman JD, Ahmed R.** 1998. Viral immune evasion due to persistence of activated T cells without effector function. J Exp Med **188:**2205-2213.

62. **Camelo S, Lafage M, Galelli A, Lafon M.** 2001. Selective role for the p55 Kd TNF-alpha receptor in immune unresponsiveness induced by an acute viral encephalitis. J Neuroimmunol **113:**95-108.

63. **Dodd KA, McElroy AK, Jones ME, Nichol ST, Spiropoulou CF.** 2013. Rift Valley fever virus clearance and protection from neurologic disease are dependent on CD4+ T cell and virus-specific antibody responses. J Virol **87:**6161-6171.